Aus der Klinik und Poliklinik im Dr. von Haunerschen Kinderspital

Klinik der Ludwig-Maximilians-Universität München

Direktor: Prof. Dr. med. Christoph Klein

Probe the transport function of ABCA3 by metabolic labelling of choline phospholipids

Dissertation
zum Erwerb des Doktorgrades der Humanbiologie
an der Medizinischen Fakultät der
Ludwig-Maximilians-Universität zu München

vorgelegt von

Yang Li

aus

Sichuan, China

2020

Mit Genehmigung der Medizinischen Fakultät
der Universität München

Berichterstatter: Prof. Dr. med. Matthias Griese

Mitberichterstatter: Prof. Dr. med. Erika von Mutius

Prof. Dr. med. Albrecht Bergner

Mitbetreuung durch den
promovierten Mitarbeiter:

Dekan: Prof. Dr. med. dent: Reinhard Hickel

Tag der mündlichen Prüfung: 17.09.2020

Content

Index of Figures

Index of Tables

Abbreviations

ABCA3	ATP binding cassette subfamily A member 3
Asn	Asparagine
ATI	Alveolar type I
ATII	Alveolar type II
BALF	Broncho-alveolar lavage fluid
CDP	Phosphocholine cytidylyltransferase
chILD	Childhood interstitial lung diseases
CHPT	Cholinephosphotransferase
CK	Choline kinase
CMP	Cytidine monophosphate
COPA	Coatomer protein complex subunit α
CTP	Cytidine triphosphate
DMSO	Dimethyl sulfoxide
DPLD	Diffuse parenchymal lung disease
DPPC	Dipalmitoyl phosphatidylcholine
ECDs	Extracellular domains
EE	Early endosomes
ER	Endoplasmic reticulum
ESI-MS/MS	Electrospray ionization-tandem mass spectrometry
FFA	Free fatty acids
GATA2	GATA-type transcription factor
Golgi	Golgi apparatus
LB	Lamellar body
LBM180	Lamellar body membrane protein

LYS	Lysosomes
Lys	Lysine
LysoPC	Lyso-phosphatidylcholine
MARS	Methionine-ARNt-synthetase
MLF	Miltefosine
MVB	Multi vesicular body
NBD1	Nucleotide binding domain 1
NBD2	Nucleotide binding domain 2
PAP	Phosphatide phosphatase
PC	Phosphatidylcholine
PE	Phosphatidylethanolamine
PG	Phosphatidylglycerol
PI	Phosphatidylinositol
propargyl-Cho	Propargyl-choline
PS	Phosphatidylserine
RDS	Respiratory distress syndrome
ROI	Region of interest
SM	Sphingomyelin
STARD10	START domain-containing protein 10
TAG	Triacylglycerols
TMDs	Transmembrane domains
TMEM173	Transmembrane protein 173
TopF-PC	TopFluor phosphatidylcholine
TTF1	Thyroid transcription factor 1

Abstract

The ATP-binding cassette sub-family A member 3 (ABCA3) plays a critical role in the lipid metabolism of pulmonary surfactant. Locating on the outer membrane of the storage and secretion compartment of surfactant in alveolar type II cells, the lamellar bodies (LBs), ABCA3 is responsible for transporting phospholipids from the cytoplasm into the LBs. Mutations of ABCA3 were identified from patients suffering from neonatal respiratory distress syndrome (RDS) and childhood interstitial lung diseases (chILD). Therefore, exploring the functional assays of ABCA3 is in great demand for pathophysiology investigation and treatment researching.

In the present study, wild type and variants of ABCA3 were expressed in A549 epithelial cells to probe mechanisms for transport activity of ABCA3. To quantify the function of ABCA3 alleles, we employed the choline analogue propargyl-Cho. Propargyl-Cho was taken up and the resultant phospholipids can be detected using a combination of click chemistry, fluorescence derivatization and microscopy to visualize and quantify the phospholipid end product. The accumulation of labeled phospholipids was time, concentration dependent. The detection of signal was dependent on choline kinase to incorporate the label into cellular phospholipids. Miltefosine, another substrate of ABCA3 can compete with the transport of propargyl-Cho. Finally, we showed that mutations (p.N568D and p.L1580P) in the ATP-binding cassette of ABCA3 impaired transport function of propargyl-Cho into intracellular vesicles.

The present thesis addressed a novel method to assess structure-function relationships of ABCA3.

1 Introduction

1.1 Pulmonary surfactant

Pulmonary surfactant is the lining mixture located on the air-liquid interface of lung alveoli space. The most critical function of the surfactant is to lower the surface tension therefore enable airway reopening at the end of exhalation. In 1929, Von Neergaard detected pulmonary surfactant by measuring pressure-volume curves in pig and dog lungs [1]. It was concluded that the lung recoil was mainly surface tension instead of tissue elastic resistance. After 30 years, Avery and Mead unraveled the cause of respiratory distress syndrome (hyaline membrane disease) was due to pulmonary surfactant deficiency [2]. Since the 1990s, surfactant replacement therapy for preterm and term neonates suffered from respiratory distress has been proved to be safe and efficient [3].

1.1.1 Synthesis of surfactant lipids

The human terminal airspace comprises two main epithelium cell types: Alveolar type I (ATI) cells and alveolar type II (ATII) cells. ATI cells are major components of the alveolar gas-exchange surface. ATII cells act as the surfactant synthesis factory, innate immune defender, and healer of lung injury. Morphologically, distinct to the large

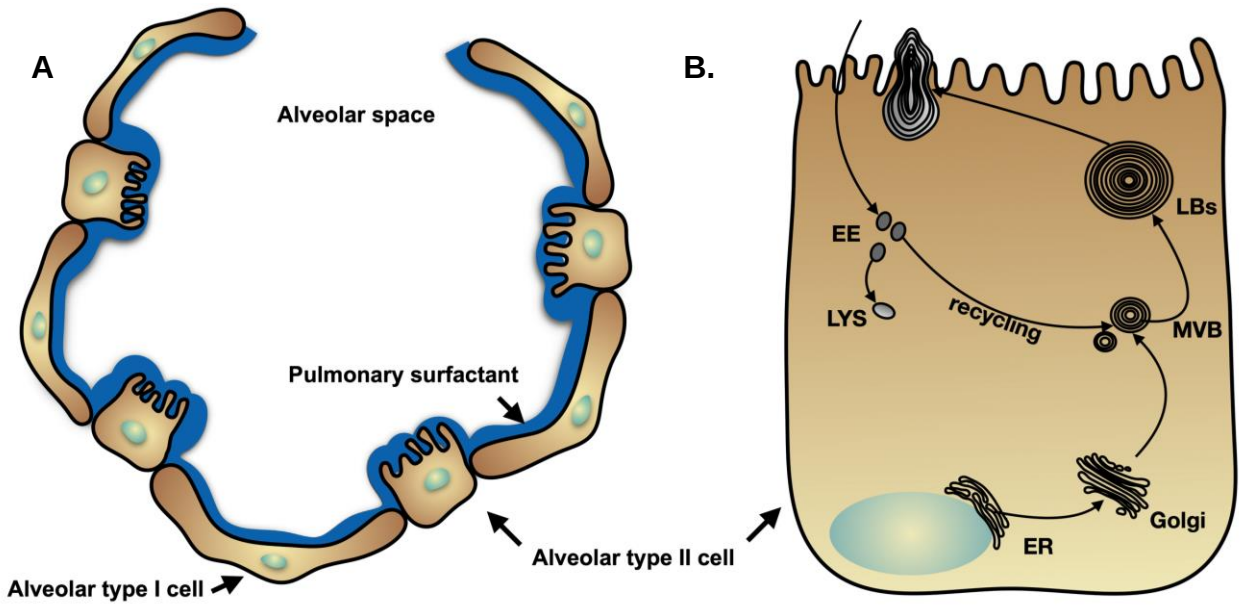

Figure 1. Alveolar epithelial cells. (**A**) Alveolar type I and type II cells. Surfactant is a thin layer of lipids and proteins mixture on the liquid-gas interface of alveolar space. (**B**) Alveolar type II cells. Biogenesis of surfactant starts from ER, routed to Golgi, MVBs and finally stored inside LBs. Surfactant secreted from LBs majorly are recycled back into ATII cells routed to LYS. ER: Endoplasmic reticulum, Golgi: Golgi apparatus, MVB: Multi vesicular body, LB: Lamellar body, LYS: lysosomes.

flat ATI cells, ATII cells are cubic and have lamellar bodies (LBs) inside and microvilli on the apical side [4] (Fig. 1).

In ATII cells, there are two *de novo* biosynthesis pathways of phosphatidylcholine (PC). The CDP - choline (Kennedy) pathway includes phosphorylation of choline to phosphocholine by choline kinase (CK), then phosphocholine is transferred into CDP - choline by phosphocholine cytidylyltransferase (CDP) and finally turned into phosphatidylcholine with the enzyme cholinephosphotransferase (CHPT) (Fig. 2). The rate-limiting enzyme in this process is CHTP, inhibition of which could lead to time and dose dependent apoptosis on exposed cells [5]. Inhibition of choline kinase by specific inhibitor could also inhibit PC synthesis [6]. The diglycerol is supplied by reaction of phosphatide phosphatase (PAP) on phosphatidic acid. By remodeling of *de novo* synthesized PC, other choline head group lipids such as lyso-phosphatidylcholine (LysoPC) and sphingomyelin (SM) are produced [7, 8].

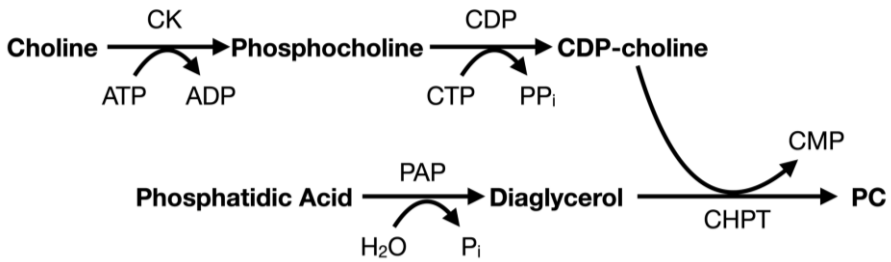

Figure 2. *De novo* pathway. Synthesis of phosphatidylcholine (PC) needs cooperation of a series of enzymes in ATII cells. CK: choline kinase, CDP: phosphocholine cytidylyltransferase, PAP: phosphatide phosphatase, CHPT: cholinephosphotransferase, CTP: cytidine triphosphate; CMP: cytidine monophosphate.

Intriguingly, alveolar type II cells not only synthesis newly phospholipids, but also recycle the secreted surfactant lipids directly from alveoli [9-11]. By instilling radioactively labeled surfactant lipids into the lungs of rabbits, Jacobs H *et al*. found that about 10% of the surfactant lipids pool in ATII cells were reutilized hourly [12]. The percentage of reutilized phosphatidylcholine could reach as much as 95% in ATII cells, and the efficiency of reutilization depended on the species of the lipid and possibly the age [12, 13]. For example, the reutilization rate of phosphatidylglycerol and phosphatidylethanolamine is slower than phosphatidylcholine [14].

1.1.2 Composition of surfactant

Lipids compose around 90% of surfactant while the other 10% is surfactant proteins. Around 80 – 90% of total lipids in surfactant are phospholipids; the rest are cholesterol, triacylglycerols (TAG) and free fatty acids (FFA) in a descending order. Of the phospholipids, around 70 – 80% are PC, the rest are phosphatidylethanolamine (PE, 12%), phosphatidylglycerol (PG, 10%), phosphatidylinositol (PI, 0.4%), lysophosphatidylcholine (LysoPC, 0.3%), phosphatidylserine (PS, 0.1%) and others (3%) [15]. The most important PC specie, dipalmitoyl phosphatidylcholine (DPPC, 16:0/16:0) consists about 50% of the total mass of surfactant, and the rest are monoenoic species such as C16:0/18:1 and C16:0/16:1, and dienoic species such as C16:0/18:2 [7, 16-18].

Around 10% of surfactant mass is proteins. Surfactant specific proteins include two hydrophilic proteins SP-A (3 – 4%) and SP-D (0.5%), and two hydrophobic proteins SP-B (0.1%) and SP-C (0.5%) [19-22]. SP-B and SP-C could accelerate the adsorption of mixed up surfactant lipids to the gas-liquid interface, and in certain circumstances the hydrophilic protein SP-A could even promote this process [23-25]. Besides related to normal surfactant physiologies, SP-A and SP-D also play roles in regulating innate

and adaptive immune functions of the host by mediating phagocytosis and discriminating against pathogens *in vivo* and *in vitro* [26, 27].

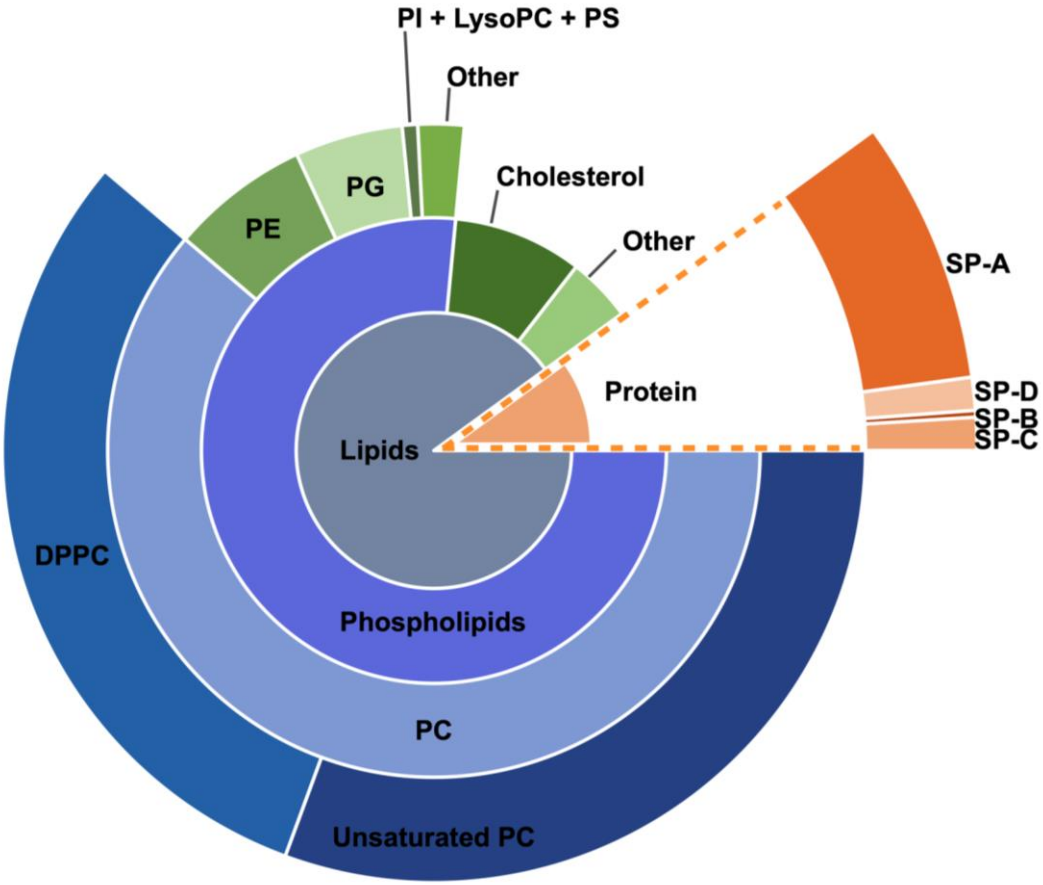

Figure 3. Lipids and protein composition of pulmonary surfactant. Phospholipids data of ATII cells were from the study of Mason and Williams [15].

1.1.3 Transport of surfactant between sub organelles

Mavis. R.D. *et al*. proved the phospholipids biogenesis in ATII cells mainly happened in the endoplasmic reticulum (ER) since more than 60% of phosphatide phosphatase enzyme was associated with ER [28]. The localization responsible for storing *de novo* synthesized and recycled surfactant lipids and re-secret surfactant into airspace is the lamellar body (LB). It was clarified that the internal transport direction of surfactant phospholipids was from high density fraction particles to lower density multivesicular bodies (MVB) and finally reach LBs. With phospholipids gradually accumulated inside LBs, the phospholipids/protein mass ratio of LBs increased [29-

31]. However, the mechanism of sorting and transporting of synthesized phosphatidylcholine from ER to LBs is not clear. Either the Golgi apparatus contributes to the transportation of PC or not is controversial. Autoradiograph results from Chevalier G and Collet AJ showed that the label [^{3}H] choline colocalized massively in the Golgi apparatus zone 30 min after in vivo injection [31]. However, by disassembling the Golgi apparatus by brefeldin A and [^{3}H] choline labeling, Osanai K and colleagues clarified the transport of phosphatidylcholine from ER to lamellar bodies was a Golgi – independent way [32, 33]. Since lamellar bodies do not possess the necessary enzymes for surfactant lipids production [28], it is not bold to presume the existence of lipids transfer protein or vesicular transportation between ER and LBs. After knocking down the START domain-containing protein 10 (STARD10) in mice [34-37], Sui L *et al*. found the saturated phospholipids in LBs decreased thus predicted STARD10 played a role in phospholipids trafficking [38].

1.1.4 Lamellar bodies

Lamellar bodies are the intracellular surfactant pool which store and secret assembled surfactant by moving to the apical surface of ATII cells. The diameter of LBs varies from 0.1 μm to 2.4 μm. In physiological conditions, LBs are vesicles assembled by multiple lipids layers, thus in a shape of ‘onion’ under electron microscope.

Originated from the lysosome, LB shares similarities with its ancestor. According to the ATP-dependent process, the internal pH of LBs is below 6.1 measured by Chander A. *et al*. [39]. LBs also contain several proteins or markers the same as lysosomes such as acid phosphatase and CD63. LBs store the phospholipids inside, meanwhile hold mature SP-B and SP-C that were transported into LBs through the Golgi-dependent pathway. Although the specific mechanism of transporting these proteins into LBs is not clarified, it could be explained that the super hydrophobic SP-

B and SP-C tend to enter LBs, which virtually are vesicular multiple lipids layer in physiological conditions.

Besides ATII cells in the lung, LBs were also found existed in the mucosa cells in the gastrointestinal tract, epidermal cells in the skin, tongue papillae and mesodermal cells in joints. Although the species of lipids inside LBs varies from the location, the principal function of LBs in situ is to produce hydrophobic protection [40-48].

1.1.5 Function of surfactant lipids

The dominant phospholipid specie in the surfactant is dipalmitoyl phosphatidylcholine (DPPC), which composes about 50% of phosphatidylcholine in ATII cells [49-52]. DPPC has the palmitic acid on both 1- and 2- positions. At the end of expiratory when the lung is at the lowest volume, DPPC could help to lower surface tension to less than 10 mN/m, thus reopen the airspace and prevent alveolar edema [53]. Although the acidic phospholipids PG and PI are only a minor proportion of surfactant, they potentially help to reduce surface tension after mixing up with DPPC [54].

1.2 ABCA3

ABCA3, short of ATP binding cassette subfamily A member 3, is a lipids transporter explicitly located on the outer membrane of lamellar bodies from the ABC transporter family. In 2002, ABCA3 was firstly identified by Mulugeta S *et al*. by immunoprecipitation with the antibody of lamellar body membrane protein of 180 kDa (LBM180) [55, 56]. With the critical role of ABCA3 in phospholipids transport was stated by in vivo and in vitro experiments [57-61], the abnormal function of ABCA3 was realized to had a causal relationship with childhood interstitial lung diseases (chILD) and RDS.

1.2.1 ABC transporter family

ABC transporters are a group of membrane proteins that exist in eukaryotes, bacteria and archaea. By hydrolyzing ATP to ADP, ABC transporters transfer alacrities against a concentration gradient across lipid membrane. It's not exaggerating to name ABC transporter family a 'super family'. To date, 48 ABC transporter genes have been identified in the human genome and divided into seven subfamilies. ABC transporters share homologous structures: two nuclear tide binding domains (NBDs, bind to ATP or ADP), and two transmembrane domains (TMDs) which commonly contain six transmembrane α-helix [62-65]. Three conserved motifs are situated in the NBDs: Walker A, Walker B and a signature motif C which locates between A and B distinguishing ABC transporters from any other ATP binding proteins [66]. Some ABC transporters are organized to have full domains of NBDs and TMDs (e.g. ABCA1, ABCA3), some possess only one set of the domains (e.g. ABCA5 and 8, ABCG2), few others even have extra domains (e.g. ABCC1).

Substrates of ABC transporters include lipids, ion, drug or drug conjugates, peptides, nucleosides and sterols. Due to the indispensable role of ABC transporters in physiological states, mutations happening to their coding gene can cause mild to severe diseases. For example, Tangier disease (ABCA1), cystic fibrosis (ABCC7), Stargardt macular degeneration (ABCA4), Dubin–Johnson syndrome (ABCC2) and interstitial lung diseases (ABCA3) [67-75].

1.2.2 Biogenesis and structure of ABCA3

ABCA3 gene in the human genome locates on chromosome 16p13.3, includes 80 kb genomic DNA and codes 1704 amino acids (NM_001089.2) [60, 76]. RNA expression of ABCA3 was found in a variety of tissues and organs while exceptionally high in lung tissue [77]. Studies from primary ATII cells and transfected cell models showed the ABCA3 biogenesis pathway in ATII cells: after synthesized in the endoplasmic reticulum (ER), ABCA3 is routed to and modified in Golgi apparatus then

sorted to multivesicular bodies (MVB), and finally directed to the outer membrane of LBs. After releasing the lipids into alveolar, ABCA3 is recycled into early endosomes (EE) and back to MVBs (Fig. 4A) [56, 59, 68, 72, 77-81].

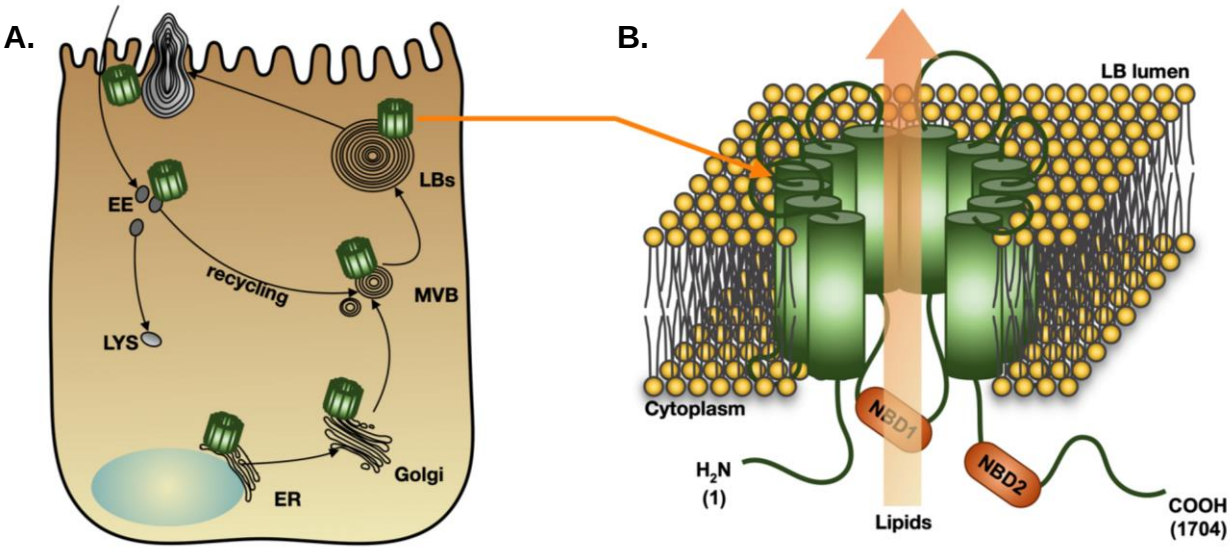

Figure 4. Biogenesis and 3D structure of ABCA3. (**A**) Biogenesis of ABCA3. The post-translational product of ABCA3 was assembled in ER, modified in Golgi and directed to MVBs and outer membrane of LBs. (**B**) 3D structure of ACBA3 on the outer membrane of LBs. Conformational change of ABCA3 made it possible to transport lipids from cytoplasm to the lumen of LBs. NBD1: nucleotide binding domain 1, NBD2: nucleotide binding domain 2.

By site directed mutagenesis of putative N-glycosylation sites in ABCA3, Beers MF *et al*. found N-glycosylation at sites Asn124 and Asn140, close to the N-terminal (Fig. 5) [81]. Deficient N-linked glycosylation of ABCA3 by inhibition with tunicamycin, or substitution of asparagine to glutamine at p.124 and p.140 resulted in ABCA3 being retained in ER and misrouted to proteasomes.

In immunoblots, wild type ABCA3 has two bands simultaneously [61, 82, 83]. In the study of Engelbrecht S *et al*., scientists found N-terminal tagged ABCA3 owned only one protein band compared to C-terminal tagged ACBA3, while consistent inhibition of protein translation would lead to the fade of the upper band [84]. Then they

blotted ABCA3 from p.Q215K mutant cells in which ABCA3 was retained in ER; the results indicated the mutant protein was lack of lower band. Finally, with immunofluorescence it was recognized that ABCA3 protein was cleaved at the N-terminal inside LAMP3+ vesicles with the protease cysteine. In a later study of the same group, the exact cleavage site of ABCA3 was proved to locate after Lys174 in the first extracellular loop (Fig. 5) [79].

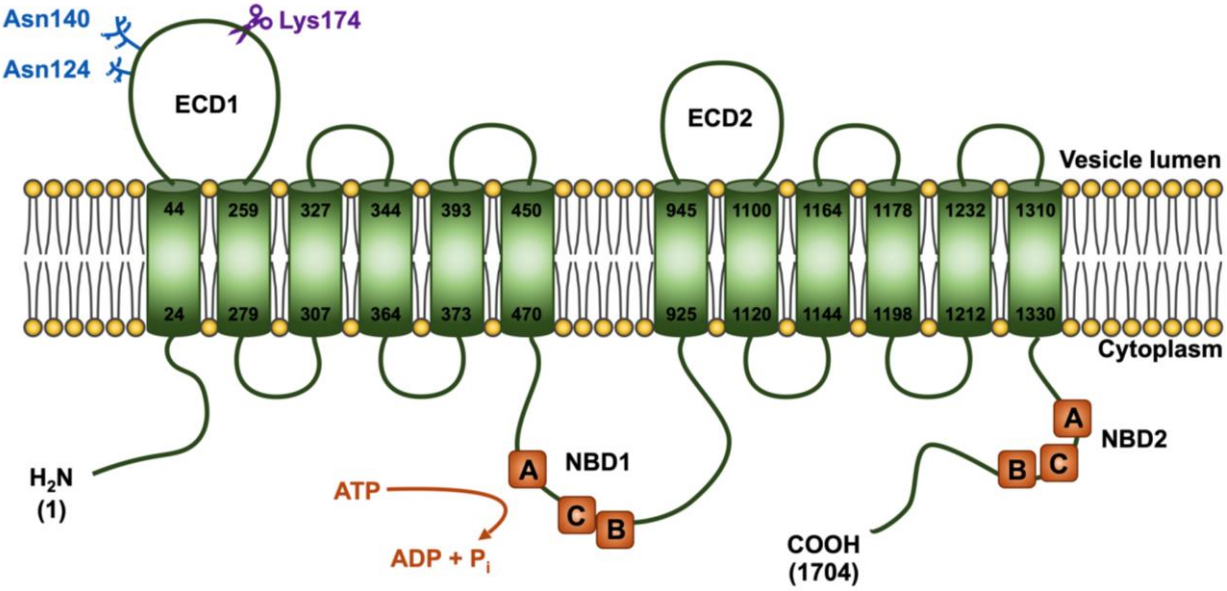

Figure 5. Ultra-structure of ABCA3. From N-terminal to C-terminal of ABCA3, lying two extracellular domains (ECD2 and ECD2), two transmembrane domains, two nucleotide binding domains (NBD1 and NBD2). A: Walker A motif, B: Walker B motif, C: signature sequence C.

Sharing common structures of ABC transporters, ABCA3 contains two NBDs facing towards the cytoplasm, two TMDs each consists of 6 transmembrane α-helix and 2 extracellular domains (ECDs), facing towards lamellar body lumen. Although due to different prediction algorithms the numbers to identify the structure of 12 transmembrane α-helix and NBDs are slightly different in studies [58, 85-87], it's consensus that each α-helix consists of 20 amino acids and the length of NBD1 and NBD2 are 153 and 154 amino acids separately (Fig. 5). Paolini A *et al*. postulated the

NBD1 spanned from aa.569 to aa.721, while NBD2 spanned from aa.1419 to 1572 in ABCA3. The region of Walker A and B motif in NBD1 were GHNGAGKT and VLILD, while in NBD2 were GFNGAGKT and VIFLD [86]. Besides Walker A and B motifs, in each NBD exists Q-, D- and H-loops, which are important among others for ATP binding, conformational change and protons shuttling between reactants. [86, 88-90].

1.2.3 Function of ABCA3

ABCA3 is key to the biogenesis of full functioning LBs in human lung. Expression of ABCA3 in A549 cells or HEK293 cells both resulted in LB-like vesicles inside. While silencing of ABCA3 in human ATII cells or rat lung cells lead to aberrant or disappearing of LBs [57, 59, 67, 72, 78, 91, 92].

Located on the outer membrane of LBs, ABCA3 is in charge of transporting a variety of lipids such as phosphatidylcholine from cytoplasm into LBs. In ABCA3 knocked out mice, normal LBs were substituted by abnormal electron dense bodies in ATII cells. Meanwhile, lipids mass spectrometry indicated PC and PG in ABCA3 knocked out lung dramatically decreased compared to normal ones [67]. Similar results were concluded from the study of Fitzgerald ML *et al*., that in ABCA3 null mice more than 300 subspecies of PG and several PC lipids were reduced compared to wild type [91]. Cheong N *et al*. found ABCA3 expression increased A549 cells uptake of sphingomyelin and cholesterol besides PC [72].

1.2.4 ABCA3 mutations and related pulmonary diseases

Since PC, PG and cholesterol are essential components of pulmonary surfactant as introduced in Part 1.1.6, the transport function of ABCA3 is indispensable for surfactant homeostasis. The fact that ABCA3 null mouse models with disrupted LBs and aberrant surfactant components died few hours after birth is a strong proof of the point [57, 58, 67, 72, 91]. Electron microscopy of the lung tissue of infants who suffered

from severe RDS with ABCA3 homozygous or compound heterozygous mutations exhibited altered ultrastructure of LBs [93-97].

Up to date, more than 200 patients' originated mutations of ABCA3 gene have been identified around the world [98]. The majority of these mutations have a phenotype of severe pulmonary surfactant deficiency. Thus patients could only survive few hours to few months after birth [96, 99-105]. In the cohort study from Wambach JA *et al*., patients with frameshift or nonsense mutation on both alleles had worse outcomes (100% chance to suffer respiratory failure at birth) compared to other homozygous or compound heterozygous genotypes (75%) [106].

ABCA3 mutations are also a major cause of childhood interstitial lung diseases (ChILD), also called diffuse parenchymal lung disease (DPLD). The pathology features of ChILD are variable and clinical manifestations include tachypnea, hypoxemia, crackles, and failure of thriving. [107]. Thus, the non-specific clinical features make it difficult to diagnose the disease by physicians. Lipids mass spectrometry analysis of broncho-alveolar lavage fluid (BALF) from ABCA3 – deficient ChILD patients showed that PC-specie with 30 and 32 carbons and almost all PG species were reduced compared to control group [49].

Genes or proteins involved in ChILD include surfactant protein families (*SFTPA*, *SFTPB* and *SFTPC*), ABCA3, thyroid transcription factor 1 (TTF1), methionine-ARNt-synthetase (MARS), GM-CSF receptors (CSF2RA, CSF2RB), GATA-type transcription factor (GATA2), transmembrane protein 173 (TMEM173) and coatomer protein complex subunit α (COPA) [108]. ChILD due to ABCA3 mutations has a prevalence of about 1.5/million per year [109]. It was prostituted that ABCA3 mutations might be the most common cause of genetic surfactant diseases although lack of systematic analysis of other inherited causes, since the number of reported cases arises every year [110, 111].

The ABCA3 genotypes leading to ChILD are commonly compound heterozygous mutations of nonsynonymous substitution. A traditional way to classify the type of ABCA3 mutations in ChILD is as follows: Type I mutation, also known as trafficking mutations, means the genetic variation leads to the misfolding or misrouting of ABCA3. Thus it is retained in the upper stream of the intracellular transportation routine, typically in the ER. Confocal microscopy of this type of mutant cells showed no mature ABCA3+ vesicles, colocalization of ABCA3 with CD63 (another LB marker) disappeared, but colocalization of ABCA3 with calnexin (ER marker) existed. Examples of such variants are p.Q215K, p.A1046E, and p.G1421R [61, 112-115]. Type II mutation, also known as functional mutations, means the mutated ABCA3 possesses normal folding or processing from ER to the outer membrane of MVBs or LBs. However, the majority of this type of mutation locate close to or inside the NBD regions and therefore they affect the normal lipid transporting function of ABCA3 by influencing the ATP or ADP binding ability of NBDs or interfering with conformational changing of the substrate tunnel [61, 87, 112]. In confocal microscopy, the mutated ABCA3+ vesicles are colocalized with LBs, however, the volume is much smaller compared to WT ABCA3. Lipid components of isolated LBs from cell models were also altered [82]. For instance, p.E292V, p.N568D and p.L1580P are type II mutations. Type III mutation also referred as compound heterozygous mutations, means combination of type I and type II mutations. Patients with type III mutations always resulted in severe phenotypes and poor outcomes. For example, the most prevalent mutation of ABCA3, p.E292V, which is a type II mutation, was frequently reported to compound interact with other type I or II mutations in ChILD patients [98].

1.2.5 Treatment of ABCA3 mutations related pulmonary disease

Although the molecular mechanism of surfactant deficiency induced by ABCA3 mutations has been deeply studied, the specific treatment of this genetic disorder is

still not available. In the case reports from physicians, therapeutic strategies of chronic ILD such as exogenous surfactant, corticosteroids (either intravenous, oral or inhalation), macrolide and hydroxychloroquine always resulted in transient or inconstant effects [116-118]. Therefore, superior and specific treatment targeting on the etiology of the mutant is urgent to be discovered.

The drug development of the mutation of CFTR (ABCC7), another ABC transporter that is the classical cause of cystic fibrosis due to impaired chloride channel has been laboriously and systematically investigated. More than 100,000 small molecules have been tested by high-throughput assay for CFTR mutation treatment [119, 120]. The effective molecules were classified into two main groups: ‘correctors’ for correcting misfolded proteins, such as VX-809 [121, 122]. And ‘potentiators’ for potentiating functional defected chloride channels, such as Ivacaftor [123, 124].

Based on that the structure of ABCA3 sharing similarities with CFTR, Kinting S *et al*. treated A549 cells stably expressing ABCA3 type I or type II mutations with the correctors and potentiators used in CFTR treatment [87, 114]. After treatment with correctors C13 or C17, immunoblotting of ABCA3-HA from trafficking mutations showed two protein bands on the gel, and in confocal microscope ABCA3-HA colocalized with CD63 vesicles. To test if the transporting function of corrected ABCA3 was restored, they half quantified the transport of TopFluor phosphatidylcholine (TopF-PC) by ABCA3 which was established before [125]. The treatment strategy of functional ABCA3 mutations by potentiators also resulted in functional improvement. The pioneer experiments gave good examples of finding new therapeutic methods for ABCA3 mutations.

1.2.6 Functional assay of ABCA3

On the way for treatment research, either by individual testing or high-throughput assay of drug libraries, it is essential to establish a reliable functional assay for the

lipids transport function of ABCA3. Matsumura Y *et al*. described the ATP/ADP binding and releasing function of NBDs by vanadate-induced radioactive nucleotide trapping [61, 78, 112]. This was also used to analyze the ATP hydrolysis function of P-glycoprotein, ABCA1, ABCC2 and other ABC transporters [126-128].

In the study of Höppner S *et al*., fluorescence labeled phosphatidylcholine TopF-PC wrapped in surfactant like liposomes was utilized as a PC analogue to study the transport function of ABCA3 [125]. The advantage of combining TopF-PC, confocal microscopy and open source image analyzing software made it convenient for application. However, the TopF-PC assay has some short comings. The somewhat

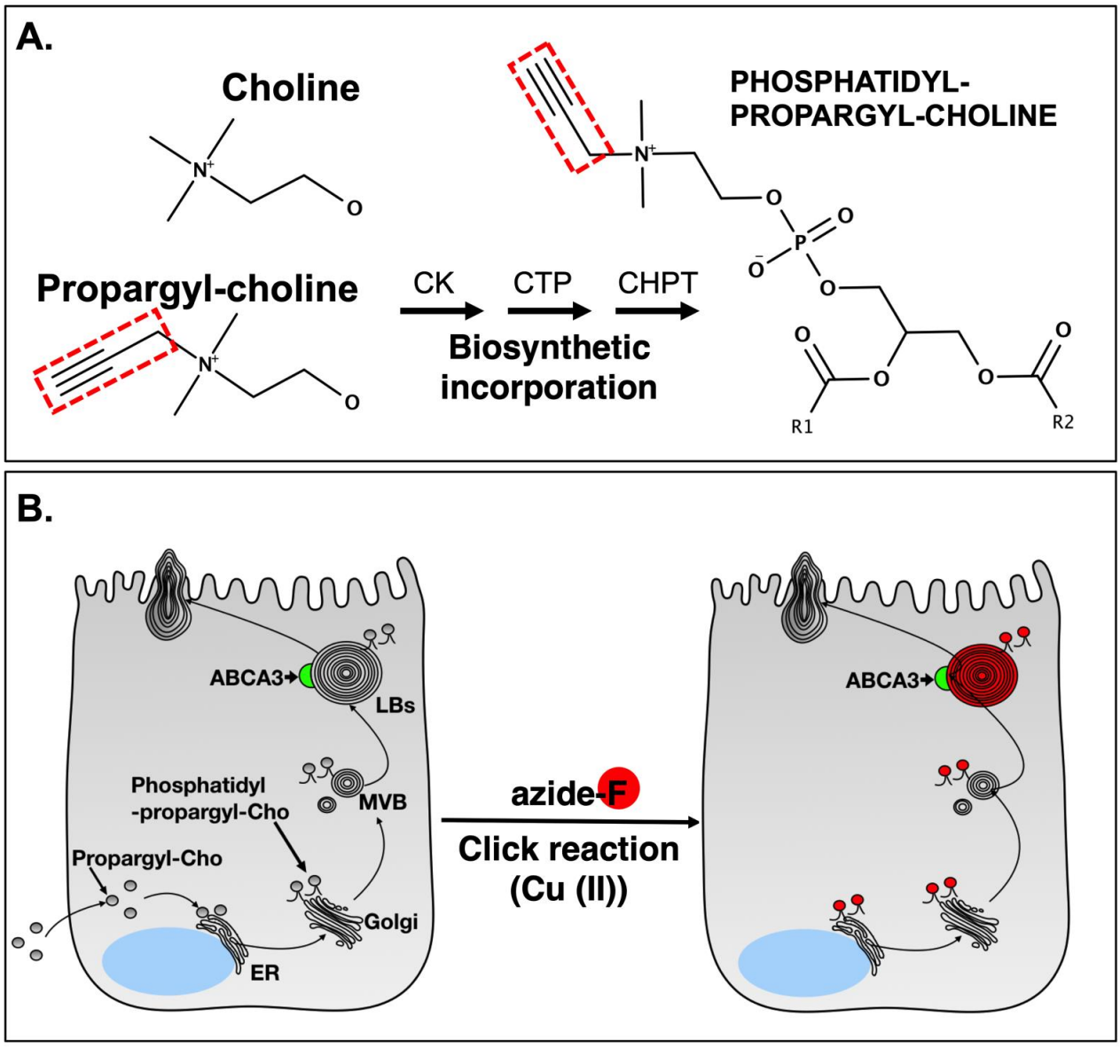

Figure 6. Propargyl-choline and click reaction of labeled PC. (**A**) Replacement of choline by propargyl-choline (propargyl-Cho) in *De novo* pathway. Structurally, propargyl-Cho has a three-carbon propargyl group (red dot box) on one methyl site of choline. Theoretically, propargyl-Cho could be transformed by series reaction of CK, CTT and CHPT into phosphatidyl-propargyl-choline. (**B**) Click reaction. After exposure, cells treated with propargyl-Cho were fixed and with the existence of Cu^{2+} labeled lipids in the cells could react with an azide fluorophore (F) and visualized by confocal microscopy together with immunofluorescence labeled ABCA3-HA. This figure is cited from Li. Y et al., 2019.

bigger size of TopF-PC compared to natural PC and the introduction of labeled liposomes into the PC-reutilization pathway made investigation of intracellular PC processing rather difficult.

Jao *et al*. reported a choline analogue, propargyl-choline (propargyl-Cho) to metabolically label phospholipids with choline head via physiological synthesis pathway (Fig. 6A). Propargyl-Cho has been successfully applied in mammalian and plant cells for the choline metabolism study [129, 130]. Based on those studies we established a new assay of choline phospholipids transport by ABCA3.

2 Aims

To establish another functional assay for the analysis of choline head phospholipids transport function of ABCA3. To determine if the choline analogue labeling assay could elucidate the transport function deviation of mutant ABCA3 protein compared to wild type. To construct a repeatable method to isolate lamellar bodies from A549 cells stably expression ABCA3 for subsequent lipidomic and proteomic studies.

3 Zusammenfassung

Die häufigste genetische Ursache für interstitielle Lungenerkrankungen im Kindesalter sind Mutationen im Gen des Lipidtransporters ABCA3. Dieser intrazellulär lokalisierte Transporter ist eine Schlüsselkomponente in der Genese der Lamellenkörperchen, dem Transport von Cholin-haltigen Phospholipiden und der Produktion von Lungensurfactant. Die Untersuchung und Quantifizierung der ABCA3-Transportfunktion spielt eine zentrale Rolle bei der Suche nach neuen Therapiemöglichkeiten von interstitiellen Lungenerkrankungen aller Altersgruppen.

Ziel der Arbeit war es eine Methode zu etablieren, die eine in vitro Bestimmung Transporterfunktion ermöglicht.

Dazu wurden die Cholin enthaltenden Phospholipide in ABCA3 stabil exprimierenden Zellen mittels Propargylcholin metabolisch markiert. Die so markierten Lipide wurden durch die Klickreaktion eines Azid-Fluorophors im konfokalen Mikroskop sichtbar gemacht. Eine Quantifizierung der Fluoreszenzintensität nur innerhalb der ABCA3+-Vesikeln, zeigte die Cholinphospholipid-Transportfunktion von ABCA3 an. Mit dieser Methode konnten wir die Funktionsabweichungen zweier krankheitsverursachender Mutationen von ABCA3, p.N568D und p.L1580P, quantifizieren. Es fand sich eine gute Übereinstimmung der Ergebnisse dieser Methode, die metabolische Markierung der Lipide nutzt, mit derjenigen, die durch primär markierte Liposomen gewonnen wurden.

Somit steht nun eine weitere Möglichkeit bereit, in einem Zellmodell exprimierte ABCA3-Mutationen zu untersuchen.

4 Material and Methods

4.1 Materials

Chemicals

(+)-Sodium L-ascorbate	Sigma-Aldrich, Taufkirchen, Germany
100% Acetic Acid	Applichem, Darmstadt, Germany
2,3-Bis-(2-Methoxy-4-Nitro-5-Sulfophenyl)-2H-Tetrazolium-5-Carboxanilide (XTT)	Sigma-Aldrich, Taufkirchen, Germany
37% Formaldehyde	Merck, Darmstadt, Germany
Agarose NEEO	Roth, Karlsruhe, Germany
Bovine Serum Albumin (BSA)	Sigma-Aldrich, Taufkirchen, Germany
Complete Protease Inhibitor Cocktail	Roche, Mannheim, Germany
Copper (II) Sulfate Pentahydrate	Sigma-Aldrich, Taufkirchen, Germany
Diazabicyclooctan (DABCO)	Merck, Darmstadt, Germany
Dimethyl Sulfoxide	Sigma-Aldrich, Taufkirchen, Germany
Dithiothreitol (DTT)	Merck Millipore, Burlington, USA
Ethylenediaminetetraacetate (EDTA)	Sigma-Aldrich, Taufkirchen, Germany
Glycerol	Sigma-Aldrich, Taufkirchen, Germany
Glycine	Sigma-Aldrich, Taufkirchen, Germany
Hydrochloric Acid	Merck, Darmstadt, Germany
LB Agar	Merck, Darmstadt, Germany
LB Broth	Merck, Darmstadt, Germany
LDS	ThermoFisher Scientific, Waltham, USA
Lipofectamine 3000	ThermoFisher Scientific, Waltham, USA
Lysotracker Blue DND-22	ThermoFisher Scientific, Waltham, USA
Lysotracker Red DND-99	ThermoFisher Scientific, Waltham, USA
Methanol	Avantor, Gliwice, Poland
Miltefosine	Cayman chemical, Michigan, USA

MN58b	AOBIOUS, Massachusetts, USA
N-(2-Hydroxyethyl)-N, N-dimethyl-2-propyn-1-aminium bromide (Propargyl-choline)	Jena Bioscience, Thuringia, Germany
Orthovanadate	Sigma-Aldrich, Taufkirchen, Germany
P3000 reagent	ThermoFisher Scientific, Waltham, USA
Phenazine Methosulfate (PMS)	Sigma-Aldrich, Taufkirchen, Germany
Saponin	Roth, Mannheim, Germany
Sodium Deoxycholate	Sigma-Aldrich, Taufkirchen, Germany
Sodium Dodecyl Sulfate (SDS)	Sigma-Aldrich, Taufkirchen, Germany
Sodium Hydroxide (NaOH)	Merck, Darmstadt, Germany
Sucrose	SERVA, Heidelberg, Germany
Syber Green PCR Master Mix	ThermoFisher Scientific, Waltham, USA
TAMRA-PEG3-Azide	Baseclick, Munich, Germany
Tris Molecular biology grade	Applichem, Darmstadt, Germany
Tris((1-hydroxy-propyl-1H-1,2,3-triazol-4-yl) methyl) amine (THPTA)	Baseclick, Munich, Germany
Triton-X 100	Sigma-Aldrich, Taufkirchen, Germany
TWEEN 20	Sigma-Aldrich, Taufkirchen, Germany

Antibody

Alexa Fluor-488 donkey anti rat	ThermoFisher Scientific, Waltham, USA
Alexa Fluor-488 goat anti mouse	Santa Cruz Biotechnology, Texas, USA
Anti HA-tag rat	Sigma-Aldrich, Taufkirchen, Germany
Calnexin C-20 goat polyclonal IgG	ThermoFisher Scientific, Waltham, USA
CD63 (H-193) rabbit polyclonal IgG	Santa Cruz Biotechnology, Texas, USA
GM130 goat polyclonal IgG	Santa Cruz Biotechnology, Texas, USA
HRP-conjugated β-actin	Santa Cruz Biotechnology, Texas, USA
HRP-conjugated goat anti rabbit	ThermoFisher Scientific, Waltham, USA

HRP-conjugated goat anti mouse	ThermoFisher Scientific, Waltham, USA
Mouse anti-Stoml 2	Proteintech, Rosemont, USA
Mouse anti-EEA1	BD Biosciences, New Jersey, USA

Kit

BCA Protein Assay Kit	ThermoFisher Scientific, Waltham, USA
High Pure RNA isolation Kit	Roche, Mannheim, Germany
peqGOLD Plasmid Miniprep Kit I	peQlab, Erlangen, Germany
Tetro cDNA Synthesis Kit	Meridian Life Science, Memphis, USA

Laboratory Instruments

4000QTRAP	AB Sciex, Darmstadt, Germany
Avanti J-E High Performance Centrifuge	Beckman Coulter, Krefeld, Germany
Biological Safety Cabinets Safe 2020	ThermoFisher Scientific, Waltham, USA
BioTek™ Eon™ Spectrophotometer	ThermoFisher Scientific, Waltham, USA
Branson 450 Digital Sonifier	G. Heinemann Ultraschall und Labortechnik, Schwäbisch Gmünd, Germany
Cellometer	Nexcelom, Massachusetts, USA
Centrifuge 5417C	Eppendorf AG, Hamburg, Germany
Centrifuge 5417R	Eppendorf AG, Hamburg, Germany
Chemiluminescence Detection Module	Raytest, Baden-Württemberg, Germany
Consort EV243 Power Supply	Merck, Darmstadt, Germany
Freezer -20 °C	Liebherr, Kirchdorf, Germany
Freezer -80 °C	ThermoFisher Scientific, Waltham, USA
Heraeus Instruments Function Line	Kendro Laboratory Products GmbH, Germany

Heraeus Multifuge 3S+	ThermoFisher Scientific, Waltham, USA
Incubation Baths 1008	GFL Gesellschaft für Labortechnik, Hannover, Germany
Intas Gel iX Imager	Royal Biotech, Brandenburg, Germany
JA-25.50 Fixed-Angle Rotors	Beckman Coulter, Krefeld, Germany
Liquid Nitrogen Tank	German-Cryo, Jücken, Germany
LSM800 system	Carl Zeiss, Oberkochen, Germany
Minicentrifuge C1301	Labnet International, New Jersey, USA
Minicentrifuge MCF-2360	LMS CO., LTD, Tokyo, Japan
Nalgene Cyro Freezing Container	ThermoFisher Scientific, Waltham, USA
Nanodrop ND-1000	ThermoFisher Scientific, Waltham, USA
New Brunswick EXCELLA E24R	Eppendorf AG, Hamburg, Germany
Optima L-80 XP Ultracentrifuge	Beckman Coulter, Krefeld, Germany
Optima TLX Ultracentrifuge	Beckman Coulter, Krefeld, Germany
ROTANTA 460R	Hettich, Tuttlingen, Germany
SW32Ti Swinging Bucket Rotors	Beckman Coulter, Krefeld, Germany
T-Gradient ThermoBlock	ALT, East Lyme, USA
TLA 110	Beckman Coulter, Krefeld, Germany
UNIVERSAL 16R (Type 1602)	HETTICH, Tuttlingen, Germany
Vortex Genie 2	Bender & Hobein, Zurich, Switzerland
Vortex Mixer 7-2020	neolab Migge, Heidelberg, Germany

Disposables

µ-Slide 8 well ibiTreat	Ibidi, Gräfelfing, Germany
4titude, FrameStar 96	Brooks Life Sciences, Massachusetts, USA
Cell counting chambers	Nexcelom, Massachusetts, USA
Cell scraper	SARSTEDT, Nümbrecht, Germany

Combitips advanced 5 ml, 10 ml	Eppendorf AG, Hamburg, Germany
CyroPure Tube 1.6 ml mix. Color	SARSTEDT, Nümbrecht, Germany
FALCON 15 ml	Corning, NY, USA
Microplate, 96 well, F-bottom, clear	Greiner Bio One, Frickenhausen, Germany
Optical Adhesive Film	ThermoFisher Scientific, Waltham, USA
Parafilm laboratory film	American National Can Co., Chicago, USA
Pipette Tip 1250 µl, 200 µl, 100 µl, 20 µl	SARSTEDT, Nümbrecht, Germany
Safe-Lock Tubes 0.5 ml, 1.5 ml, 2.0 ml	Eppendorf AG, Hamburg, Germany
Single use filter Non-pyrogenic 0.20 µm	Sartorius AG, Göttingen, Germany
Stripette 50 ml, 25 ml, 10 ml, 5 ml	Corning, NY, USA
Syringe 1 ml	Becton Dickinson S.A, Madrid, Spain
Syringe 50 ml	B. Braun, Melsungen, Germany
TC-Platte 6 / 96 Well, Cell +, F	SARSTEDT, Nümbrecht, Germany
Tube 10 ml 100x16PP+Cap YLW	SARSTEDT, Nümbrecht, Germany

Cell types

A549	DSMZ, Braunschweig, Germany

Cell culture medium and materials

12 well flat bottom cell culture cluster	Corning, NY, USA
Dulbecco's Phosphate Buffered Saline	Sigma-Aldrich, Taufkirchen, Germany
Flask T75, T25	Corning, NY, USA
GlutaMAX - I (100X)	ThermoFisher Scientific, Waltham, USA
Opti-MEM (1X)	ThermoFisher Scientific, Waltham, USA
Sodium pyruvate 100mM (100X)	ThermoFisher Scientific, Waltham, USA

TC Dish 150, Standard	SARSTEDT, Nümbrecht, Germany
Tissue Culture Dish 100 x 20 mm	Corning, NY, USA
Trypsin - EDTA solution	Sigma-Aldrich, Taufkirchen, Germany

Western Blot materials

Novex Sharp Pre-Stained Protein Standard	ThermoFisher Scientific, Waltham, USA
Novex, XCell II Blot Module	ThermoFisher Scientific, Waltham, USA
NuPAGE 3-8% Tris-Acetate Gel 10 well	ThermoFisher Scientific, Waltham, USA
NuPAGE 3-8% Tris-Acetate Gel 12 well	ThermoFisher Scientific, Waltham, USA
NuPAGE Transfer Buffer (20X)	ThermoFisher Scientific, Waltham, USA
PVDF membrane	Millipore, Billerica, USA
Tris-Acetate SDS Running Buffer (20X)	ThermoFisher Scientific, Waltham, USA

Buffers and Solutions

RIPA (Radioimmunoprecipitation assay) buffer

Tris	50 mM
SDS	0.1 % (v/v)
Triton-X 100	1 % (v/v)
EDTA	5 mM
NaCl	0.15 M
Sodium deoxycholate	0.5 %
Complete protease inhibitor cocktail	1 x
pH	8.0

TBS-T

Tris	50 mM
NaCl	0.15 M

Tween 20	0.1 % (v/v)
pH	7.5

TAE buffer (10x)

Tris	0.4 M
Glacial acetic acid	0.2 M
EDTA	0.01 M
pH	8.5

PBS-Glycine

Tris base pH 8.5	0.4 M
Glacial acetic acid	0.2 M
EDTA	0.01 M

Mounting media

Glycerol	90% (v/v)
DABCO	2% (w/v)

Immunofluorescence (IF) buffer

BSA	3% (w/v)
FBS	3% (w/v)

Immunofluorescence – Saponin (IF-S) buffer

BSA	3% (w/v)
FBS	3% (w/v)
Saponin	0.5% (w/v)

PBSBS washing buffer

BSA	0.01% (w/v)
Saponin	0.1% (w/v)

CuAAC reaction Buffer

BSA	0.01% (w/v)
Saponin	0.1% (w/v)
Sodium ascorbate	1.2 mM
THPTA	128 µM
TAMRA-Azide	20 µM
$CuSO_4$	1 mM

Sucrose Tris buffer

Tris	20 mM
Sucrose	1 M
pH	7.3

DAPI nuclear staining buffer

DAPI	0.1 µg/ml

4.2 Methods

4.2.1 Site directed mutagenesis

Transposon vector contains ABCA3 template DNA (pT2/HB-CMV-hABCA3-HA-PGK-Puromycin) was from the study of Wittmann, T *et al*. [131]. p. N568D (c. 2886A>G; CAA/CGA) or p.L1580P (c.5923T>C; CTG/CCG) point mutations were introduced into the template with Q5® Site-Directed Mutagenesis (SDM) Kit. Forward and reverse primers of these two mutations were listed as in Table 1. According to the SDM kit protocol, a 25 µl reaction system containing 25 ng template DNA, 0.5 µM forward and reverse primers and nuclease-free water were mixed up thoroughly. Routine PCR cycling condition of the reaction system: initial denaturation at 98°C for 30 sec, 25 cycles of denaturation (98°C, 30 sec) – annealing (Ta of target primers, 30 sec) – extension (72°C, 5 min 45 sec), and final extension at 72°C for 2 min. Treat 1 µl of PCR product with kinase, ligase and Dpnl (KLD) enzyme mix (provided in the kit) at room temperature for 5 min to digest template DNA.

Table 1. Point mutagenesis primers

ABCA3-mutation	Forward primer (5'-3')	Reverse primer (5'-3')
p. N568D	GCTGGGCCACGACGGTGCCGG	AGGACGGTGATCTGTCCCTCGTACAG
p. L1580P	TGTGAGGCCCCGTGCACCCGG	CTCCTCCATGCTGTGGGAGG

For transformation, add 5 µl of KLD mix into a tube of 5-alpha Competent *E. coli* cells, mix thoroughly and incubate on ice for 30 min. Then the mixture was processed to heat shock at 42°C for 30 sec and cooling down on ice for 5 min. Add SOC medium to the mixture and shake (250 rpm) for 60 min at 37°C for amplification. Spread 50 µl of amplified cells on the selection lysogeny broth (LB) agar plate (Ampicillin 100 µg/ml)

and incubate overnight. For each mutation, pick 10 clones and incubate overnight with 6 ml Ampicillin – LB medium in falcons.

4.2.2 Plasmid preparation

Centrifuge transformed *E. coli* cells in the falcon down at 4600 g, at 4°C for 15 min. Isolate DNA with peqGOLD Plasmid Miniprep Kit I according to the instruction. Briefly, resuspend bacterial pellet with 250 µl Solution I/RNase A, add the same amount of Solution II, mix carefully until the lysate get cleared and let stand 2 min in room temperature. Next, neutralize the lysate by adding 350 µl Solution III in the kit which will immediately form a white flocculent precipitate. Centrifuge the mixture at 10.000 g, 10 min. Load the clear supernatant to a new DNA column in a collection tube. Centrifuge the device for 1 min at 10.000 g and discard the liquid. Then add 500 µl PW buffer once, 750 µl DNA wash buffer twice for in total three times of wash. Between each wash step, centrifuge for 1 min at 10.000 g. After wash, dry the column matrix by centrifuge the collection tube again at 10.000 g for another 2 min. Discard the tube and insert the column into a fresh 1.5 ml centrifuge eppi, add 50 µl elution buffer and centrifuge at 5000 g to elute DNA. Measure the DNA concentration with Nanodrop.

4.2.3 Agarose gel electrophoresis

Add 1 g agarose in 105 ml TBE buffer in 250 ml wide-mouth flask. Heat the mixture up in microwave at 800 w for 3 min 30 sec. Carefully handle the heated flask with insulation gloves to flowing water until the mixture cooling to hand warm. Add 15 µl ethidium bromide solution and mix gently. Resemble UV-transparent tray, two end gates and a comb together, pour the cooled down liquid into the system and stand in room temperature for 1 hour until firm gel formed. In each electrophoresis, 4 µl 1 kb DNA ladder was loaded together with probes. Electrophoresis setting: 120 V, 110 mA, 20 W, 45 to 50 min.

4.2.4 Sequencing

Premix 500 ng purified plasmid DNA with 5 µl of 25 ng/µl pT2/HB-CMV-hABCA3-HA-PGK-Puromycin template DNA. Add 5 µl of 5 µM sequencing primer (Table 2) into the sample. All the sequencing was done by Eurofins Genomics Germany GmbH.

Table 2. Sequencing primers

SeqPrimer	
CMV-Forward	5'-CGCAAATGGGCGGTAGGCGTG-3'
SeqABCA3#1	5'-AGCACCCCTTCAACCAC-3'
SeqABCA3#2	5'-TCGCCATCTCTACCATC-3'
SeqABCA3#3	5'-GGACGGGCATACATCAG-3'
SeqABCA3#4	5'-GGGGCATCCATCACCAC-3'
SeqABCA3#5	5'-ACGCCTCCATTGTGGTC-3'
SeqABCA3#6	5'-GCGCCTACCTCATCCTG-3'
SeqABCA3#7	5'-GCCACATGCCAACAAGC-3'
HA Seq forward	5'-CCTTGACCCTGGAAGGTGCC-3'
PKG Puro forward	5'-CTTCGCCGCTACCCTTGTGG-3'
PKG Puro reverse	5'-CCCCTCGAGGCTAGC-3'
M13-RP	5'-CAGGAAACAGCTATGACC-3'

4.2.5 Transfection and single clone generation

Human A549 cells were seeded 200,000 cells/ml in 6-well plate and maintained at 37°C and 5% CO_2. After 24 hours (or cells reach 80% confluency), mix 7.5 µl Lipofectamine 3000 reagent in 125 µl OptiMEM in microcentrifuge tube A. In tube B, prepare 4 µg DNA (2857.14 ng plasmid with confirmed sequence, 1142.86 ng transposase SB100) and 8 µl P3000 reagent in 125 µl OptiMEM. Mix the reagents in tube A and B by pipetting and incubate at room temperature for 5 min. Evenly distribute the mixed reagents on the cells. After 48 hours change the medium to puromycin containing RPMI to select successfully transfected cells. Change fresh medium every four to five days until un-transfected cells were dead. Harvest transfected cells and

seed 1 cell/well in 96-well plates. Amplify the cells with single colony developed in 12-well plates, 6-well plates, T25 and T75 flasks consistently.

4.2.6 Cell culture

Transfected A549 cells were incubated in RPMI 1640 medium supplemented with 10% fetal calf serum (FCS) and 0.02% puromycin. Wash cells with PBS. Then, treat cells with 1X Trypsin-EDTA for cell detachment. Cells were incubated at 37°C and 5% CO_2 until reached 90% confluency for downstream use.

4.2.7 BCA assay

Collect cell sample in 1.5 ml Eppi, centrifuge at 300 g for 5min. Discard the supernatant and wash cell pellets twice with PBS, then store the pellets in -20°C or resuspend in 100 µl RIPA buffer with 1X proteinase inhibitor complex on ice for 30 min. Then centrifuge the cell lysate for 30 min at 4000 g, 4°C and collect the supernatant. Dilute the protein sample with the same volume of RIPA buffer. Then add 12.5 µl of BCA protein standard (prepared in RIPA buffer according to the manufacture protocol) and diluted sample in duplicates in 96-well-plate. In each well, add 100 µl of mixed BCA assay buffer (reagent A: B, 50:1) then incubate at 37°C for 30 min. The concentration of protein was measured with a spectrometer at 562 nm.

4.2.8 Western blot

Western blot probes were prepared by mixing 15 µg protein with 10% DTT, 1X LDS and added up with distilled water to a final volume of 25 µl. Then the probes were heated up to 70°C for 10 min to reduce disulfide bonds. In the meantime, prepare 1X Tris-Acetate running buffer and 3-8% Tris-acetate gel in a prepared chamber. Add 7 µl of pre-stained protein standard and heated samples in the pockets carefully and run at 150 V, 125 mA for 80 min. During gel running, activate PVDF membrane by rinsing in 98% methanol for 1 min. Blotting was done in a wet-transfer module (XCell II Blot Module) under 125 v, 220 mA at 4°C for 120 min. Block blotted membrane in 5% defat

milk in TBS-T buffer for at least 30 min. Anti - ABCA3-HA (rat), EEA1 (mouse), Calnexin (goat), GM130 (goat) and Stoml2 (mouse) first antibodies were diluted 1:1000 in 5% milk and could be used repeatedly for 10 times. Anti – β-actin HRP conjugated (mouse) antibody was diluted 1:10000. Secondary antibodies such as anti – rat HRP conjugated (donkey), anti – mouse HRP conjugated (goat) and anti – goat HRP conjugated (mouse) were diluted 1:10000 freshly in 5% milk in single experiments. Incubating of the membranes with first antibodies for 120 min at room temperature or overnight at 4°C, and secondary antibodies for 1 h in room temperature. After each incubation, wash the membrane with 3 times of TBS-T, 5 – 10 min each. Develop the membranes with Western Blot enhancer in an illumination detector. All the images of western blot were analyzed with ImageJ.

4.2.9 cDNA synthesis

RNA of cultured cells was isolated with RNA isolation kit according to the protocol. Briefly, cells pellets were resuspended in 600 µl of 66.7% lysis buffer in PBS and thoroughly mixed by vortex. Assemble high pure filter tubes, add the mixed sample to the filter tube and centrifuge at 8000 g for 15 s. Discard the liquid on the bottom, add 10 µl DNase I and 90 µl DNase incubation buffer and incubate for 15 min at room temperature. Then add 500 µl wash buffer I to the filter tube and centrifuge at 8000 g for 15 s. Discard the liquid then wash twice with wash buffer II, dry the filter tube by a final centrifuge at 13000 g for 2 min. Elute the RNA with 50 µl elution buffer and measure the concentration with Nanodrop.

cDNA was synthesized according to Tetro cDNA synthesis kit protocol. Mix 5 µg target RNA, 1 µl random hexamer, 1 µl dNTP, 1 µl RNase inhibitor, 1 µl reverse transcriptase and add up with DEPC-treated water to a final volume of 20 µl. Incubate the samples at 25°C for 10 min followed by 45°C for 30 min, then at 85°C for 5 min and chilled at 4°C.

4.2.10 Quantitative polymerase chain reaction

Prepare paired primer mix of 25 µM forward and reverse primer. Then add 0.32 µl primer mix, 4 µl cDNA (1:5 diluted), 10 µl Syber Green Master mix and 5.68 µl ddH_2O to 96-well plates. HRPT1 was set as internal reference. Primers of qPCR were listed in Table 3. Run qPCR on an ABI 7900HT cycler with the standard curve from previous study [83, 132]. mRNA expression level was analyzed with ΔΔCt method. The expression level of mock cells was set as blank and the data from mutants were compared to wild type ABCA3.

Table 3. qPCR primers

Gene name	Forward primer (5'-3')	Reverse primer (5'-3')
ABCA3	CATGGTCAGCACCTTCTTCA	TTCTGGCTCAGAGTCATCCA
HRPT1	GCTGACCTGCTGGATTAC	TGCGACCTTGACCATCTT

4.2.11 Propargyl-choline treatment

1 mg of Propargyl-choline (propargyl-Cho) was purchased from Jena Bioscience. Add 156 µl of PBS to prepare a 50 mM stock solution of propargyl-Cho. Seed transfected A549 cells 200,000 cells/well in 8-well µ-slides and incubate overnight at 37°C and 5% CO_2 until reach 80% confluency. To treat cells with propargyl-Cho, cool the cells down at 4°C for 15 min. Dilute stock solution with ice cold OptiMEM to target concentration freshly before each experiment. Remove medium on the cells and pulse chase with 250 µl of propargyl-Cho at 4°C. After 30 min, replace propargyl-Cho with room temperature OptiMEM and incubate at 37°C. In concentration dependent tests, cells were treated with 0, 10 µM, 50 µM, 125 µM and 250 µM propargyl-Cho for 24 h. In time dependent experiments, cells were treated with same concentration (125 µM) of propargyl-Cho for different time period. To explore if single mutation of ABCA3 would lead to aberrant lipids transport function of ABCA3, p.N568D, p.L1580P and WT –

ABCA3 – HA expressing A549 cells were treated with the same concentration of propargyl-Cho for same time period.

4.2.12 Inhibitors

To characterize if the ABCA3 transportation of propargyl-Cho labeled lipids dependent on ATP consuming, cells pulse chased with 125 µM propargyl-Cho for 30 min were treated with 12.5 mM orthovanadate for 2 h and incubated for another 22 h consistently. To understand the lipids synthesis and transportation during the metabolic labeling process, cells were treated with 10 µM MN58b or 10 µM Miltefosine diluted in dimethyl sulfoxide (DMSO) at 0 h or 12 h after incubation with propargyl-Cho. Cells were washed gently with 37°C PBS for 3 times after inhibition then incubated in OptiMEM until harvested in washout experiments.

4.2.13 Immunofluorescent staining

Fixation and permeabilization of cells and immunostaining of ABCA3-HA protein were done according to established protocol [114, 115]. Briefly, wash cells twice with 200 µl PBS and fix with 3.7% formaldehyde for 20 min, then remove formaldehyde and quench the fixation by incubating with PBS-Glycine (0.1 M) for 10 min. Incubate cells with 150 µl 1% saponin to permeabilize cell membranes for 5 min and wash 3 times with PBSBS washing buffer, 5 min each. Then incubate cells with IF-S buffer for 30 min to block unspecific antigens. Cells were incubated with 1:200 diluted first antibody (anti-HA from rat) for 1 h and secondary antibody (Alexa-Fluor 488 donkey anti rat) for 30 min after blocking. Stain cell nuclei with DAPI for 20 min.

4.2.14 Click reaction

Prepare 40 mM 5-TAMRA-PEG3-Azide and 200 mM THPTA stock solution in DMSO. Prepare 100 mM $CuSO_4$ and 0.25 M sodium ascorbate stock solution in ddH_2O. Mix CuAAC reaction system freshly: 1966.2 µl PBS containing 0.01% BSA and 0.1% saponin, 9.6 µl sodium ascorbate (final concentration: 1.2 mM), 1.28 µl THPTA (final

concentration: 128 µM), 1 µl 5-TAMRA-PEG3-Azide (final concentration: 20 µM) and 20 µl $CuSO_4$ (final concentration: 1 mM). After nuclei staining, incubate cells with 240 µl of the mixture for 30 min in dark. Then wash 9 times (5 min each) with wash buffer and mount with mounting buffer. Store the samples at 4°C.

4.2.15 Imaging

A Carl Zeiss LSM800 system was used for all confocal imaging. To start, open 'ZEN' software and select channels match the fluorophores in cells. For propargyl-Cho analyzing, TAMRA (excitation: 561 nm, red), AF488 (excitation: 488 nm, green) and DAPI (excitation: 405 nm, blue) tracks were selected. In every independent experiment, laser power, pinhole, digital offset and digital gain for AF488 and DAPI channels could be adjusted for better image, while settings of TAMRA should be unchanged once settled at the beginning of that experiment. To analyze the fluorescence intensity of labeled lipids in ABCA3+ vesicles, three Z-stacks of 5 slices (0.4 µm interval) were composed in one well. The image size of the snaps and Z-stacks was 1024 x 1024 pixels. All the experiments were performed in duplicates and repeated for three times.

4.2.16 Fluorescence intensity analyzing

Fiji software and a Fiji-plugin 'Particle_in_Cell-3D' developed by Torrano AA *et al*. [133] were utilized for fluorescence intensity analyzing of Z-stacks [87, 114, 125]. After open a Z-stack file with Fiji, split the channels and run the first macro 'vesicles.ijm' to generate 'vesicles.tiff' from green channel and 'lipids.tiff' from red channel. Adjust the brightness/contrast of 'vesicles.tiff' until the edge of vesicles was sharp, select 20 random vesicles with oval tool as region of interest (ROI). To analyze the fluorescence outside of the vesicles, 20 ROIs of size 1 µm x 1 µm were draw with rectangular tool on 'vesicle – nucleus' merged images, the 'lipids' channel was not included to avoid bias. The ROIs out of vesicle should be draw in cells within ABCA3+ vesicles but without overlapping with nucleus or ABCA3+ vesicles. Fig. 7 gives an example of ROI

selection. Afterwards, fluorescence intensity was analyzed by running the second macro 'Particle_in_Cell-3D_v4.ijm' on 'lipids.tiff'. During this process, set the 'background to be subtracted value' to 0. Required data was analyzed in Excel.

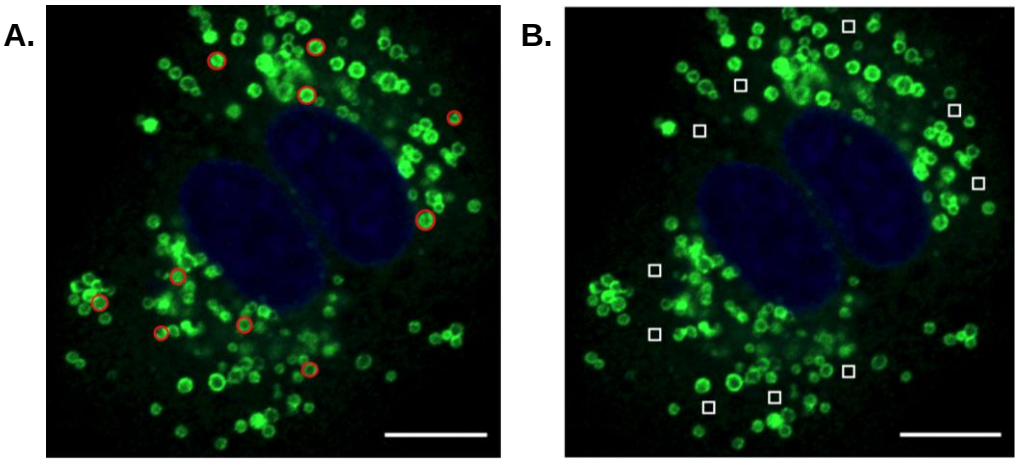

Figure 7. Region of interest (ROI). (**A**) Ten ROIs inside vesicles were marked with red and elliptical. The rules of ROI selection followed the description of Höppner et al. The edge of each ROI should overlay with the outline of the vesicle. (**B**) Ten ROIs out of vesicles (white, square) were marked as example. Scale bar: 10 µm. The figures were cited from Li Y et al., 2019.

4.2.17 Cytotoxicity assay

The effect of propargyl-Cho and inhibitors on cell viability was tested with XTT assay [83, 131]. Dilute cells to 500,000 cells/ml in phenol red free RPMI supplemented with 10% FCS. Seed 100 µl of diluted cells in 6 replicates in 96-well plates and incubate overnight. Then thaw prepared XTT solution aliquot (1 mg/ml in phenol red free RPMI medium) in 37°C water bath. Add 1.25 µl 100 mM PMS (N-methyl-dibenzopyrazine methylsulfate) solution (0.0153 g of PMS in 500 µl of PBS) in 5 ml warmed up XTT solution and mix well by pipetting. Then put 50 µl/well of mixed solution on the cells immediately after preparation and incubate at 37°C for 30 min, light proofing. Absorbance was measured at OD490 nm with a spectrometer and the background of 96-well plates (OD650 nm) was subtracted.

4.2.18 Lipids Mass-spectrometry

To ensure the incorporation of propargyl-Cho into choline head phospholipids, cells were treated with or without 100 µM propargyl-Cho for 30 min in 4°C and incubate in OptiMEM at 37°C for another 24 hours. Cell pellets were extracted by methanol including 1-tridecanoyl-2-hydroxy-sn-glycero-3-phosphocholine and 1,2-dimyristoyl-sn-glycero-3-phosphocholine (Avanti Polar Lipids, Alabaster, USA) as internal standards. With liquid chromatography coupled to a triple quadrupole mass spectrometer (1200 HPLC Agilent, Waldbronn, Germany coupled to 4000QTRAP Sciex, Darmstadt, Germany), a flow-injection analysis was performed with the mobile phase of 76% isopropanol, 19% methanol and 5% water and the flow rate of 240 µL/min. Fragments of phosphatidylcholines (m/z = 184 Da) or propargyl-Cho (m/z = 208 Da) were detected in precursor-ion-scan and mass transitions were given in Table 3. Analyzed compounds: diacyl-phosphatidylcholines (PC.aa.Cxx.y), sphingomyelins (SM.C18.1.Cxx.y) and acyl-lyso-phospholipids (lyso.PC.a.Cxx.y). Cxx.y stands for lipid side chain; xx and y indicate the number of carbon atoms and double bonds, respectively. This approach was not appropriate to specify the site of the double bonds and the arrangement of carbon atoms inside chains of the fatty acid molecule.

Table 4. Mass transitions for propargyl-Cho species

Name	Q1/Q3 phosphatidylcholines	Q1/Q3 phosphatidyl-propargyl-Cho
lyso.PC.a.C14.0	468.300 / 184.000	492.300 / 208.000
lyso.PC.a.C16.0	496.300 / 184.000	520.300 / 208.000
lyso.PC.a.C18.2	520.300 / 184.000	544.300 / 208.000
lyso.PC.a.C18.1	522.300 / 184.000	546.300 / 208.000
lyso.PC.a.C18.0	524.300 / 184.000	548.300 / 208.000
SM.C18.1.C14.0	675.500 / 184.000	699.500 / 208.000
SM.C18.1.C16.1	701.500 / 184.000	725.500 / 208.000
SM.C18.1.C16.0	703.500 / 184.000	727.500 / 208.000

SM.C18.0.C16.0	705.500 / 184.000	729.500 / 208.000
SM.C18.1.C18.2	727.600 / 184.000	751.600 / 208.000
SM.C18.1.C18.1	729.600 / 184.000	753.600 / 208.000
SM.C18.1.C18.0	731.600 / 184.000	755.600 / 208.000
SM.C18.1.C20.2	755.600 / 184.000	779.600 / 208.000
SM.C18.1.C20.1	757.600 / 184.000	781.600 / 208.000
SM.C18.1.C20.0	759.600 / 184.000	783.600 / 208.000
SM.C18.1.C22.2	783.600 / 184.000	807.600 / 208.000
SM.C18.1.C22.1	785.600 / 184.000	809.600 / 208.000
SM.C18.1.C22.0	787.600 / 184.000	811.600 / 208.000
SM.C18.1.C24.2	811.700 / 184.000	835.700 / 208.000
SM.C18.1.C24.1	813.700 / 184.000	837.700 / 208.000
SM.C18.1.C24.0	815.700 / 184.000	839.700 / 208.000
SM.C18.1.C26.2	839.700 / 184.000	863.700 / 208.000
SM.C18.1.C26.1	841.700 / 184.000	865.700 / 208.000
SM.C18.1.C26.0	843.700 / 184.000	867.700 / 208.000
PC.aa.C30.0	706.500 / 184.000	730.500 / 208.000
PC.aa.C32.1	732.600 / 184.000	756.600 / 208.000
PC.aa.C32.0	734.600 / 184.000	758.600 / 208.000
PC.aa.C34.3	756.600 / 184.000	780.600 / 208.000
PC.aa.C34.2	758.600 / 184.000	782.600 / 208.000
PC.aa.C34.1	760.600 / 184.000	784.600 / 208.000
PC.aa.C34.0	762.600 / 184.000	786.600 / 208.000
PC.aa.C36.4	782.600 / 184.000	806.600 / 208.000
PC.aa.C36.3	784.600 / 184.000	808.600 / 208.000
PC.aa.C36.2	786.600 / 184.000	810.600 / 208.000
PC.aa.C36.1	788.600 / 184.000	812.600 / 208.000
PC.aa.C36.0	790.600 / 184.000	814.600 / 208.000
PC.aa.C38.6	806.600 / 184.000	830.600 / 208.000
PC.aa.C38.5	808.600 / 184.000	832.600 / 208.000
PC.aa.C38.4	810.700 / 184.000	834.700 / 208.000
PC.aa.C38.3	812.700 / 184.000	836.700 / 208.000
PC.aa.C38.2	814.700 / 184.000	838.700 / 208.000
PC.aa.C38.1	816.700 / 184.000	840.700 / 208.000

PC.aa.C38.0	818.700 / 184.000	842.700 / 208.000

4.2.19 Cell homogenization

WT ABCA3-HA A549 cells from sic of 150 mm culture dishes (around 10^8 cells in total) were washed 3 times with room temperature PBS. Rinse cells in ice cold PBS containing 1X proteinase inhibitor complex, 1 ml/dish. Following steps were all on ice or in a cold room to chill samples. Carefully detach cells off the wall by scraping and gather cell suspensions in a 10 ml falcon. Pellet the cells down by centrifuge at 300 g for 10 min (4°C) and resuspend cells in 2 ml of 1 M Sucrose-Tris buffer (1 X PI, pH 7.3) by pipetting up and down with a tip-cut pipette. Avoid of air bubbles formation.

To homogenize cells by nitrogen cavitation, clean the vessel and micro stir bars with distilled water. After the sample outlet was tightly locked, transfer well suspended cells into the vessel. Set the vessel firmly on a stirrer with a proper stirring speed, close the cap and tighten the gas inlet and outlet valves. Afterwards, pressurize the vessel with nitrogen gas to 800 psi (pounds per square inch) and equilibrate for 10 min. Open the sample outlet valve gradually and collect the drops of cell lysates with a new falcon.

All the sonification was conducted on ice. Sonicate cells in 1 M Sucrose-Tris buffer for 3 times of 2 sec pulse, 30 sec pause and 20% amplitude. Incubate cell lysates with 5% formaldehyde for 20 min. Get rid of unbroken cells or big debris by centrifuge at 1000 g for 10 min. The post nuclear supernatant (PNS) was diluted with 1 M Sucrose-Tris buffer until the total volume of PNS reached 5 ml. Save 0.5 ml PNS for Bradford assay and western blot, and the rest 4.5 ml for sucrose gradient LBs isolation.

4.2.20 Mark lamellar bodies with Lysotracker Red

To prepare samples for fluorescence activated lamellar bodies sorting, WT ABCA3-HA cells were cultured in 150 mm culture dishes until 90% confluences. Prepare 100 nM Lysotracker Red (LTR) in 37°C DMEM (1 µl of 1 mM LTR stock

solution in 10 ml DMEM). Incubate cells with 15 ml of 100 nM LTR or merely medium (control) at 37 °C, 5% CO2 for 1 h then wash out LTR with PBS. Fixing cells with 3.7% formaldehyde, statin ABCA3-HA with anti – HA antibody. Verify the uptake of LTR into LBs by confocal microscope.

4.2.21 Lamellar body isolation

Protocol for lamellar body isolation was improved from previous studies. Briefly, add 3.5 ml PNS from homogenization on the bottom of a new 30 ml ultracentrifuge tube. On top of PNS, add 1 ml of 0.8, 0.7, 0.6, 0.5, 0.4 and 0.3 M sucrose sequentially. Finally, pipette 0.5 ml 0.2 M sucrose solution on top. Avoid of bubbles or vibration in the process. After balancing, samples were centrifuged for 15 min at 138 g and 4 h at 80428 g without interval in between. Collect fraction 1 to 10 from top to bottom with fine tips, 1 ml per fraction.

4.2.22 Statistical analysis

Rough data from individual experiments were anazyed with Microsoft Excel and further processed with Prism 8. One- or Two-way ANOVA and t-test were used in grouped data analyzing. For multiple comparisons in two-way ANOVA, Tukey, Dunnett or Sidak correction test were conducted.

5 Results

5.1 Establish an assay to probe the phosphatidyl-choline transport function of ABCA3

5.1.1 Construction of ABCA3-HA stable expressing cells

Western blot and qPCR were used to confirm the successful transfection and stable expression of ABCA3-HA in A549 cells. Similar to WT, N568D and L1580P

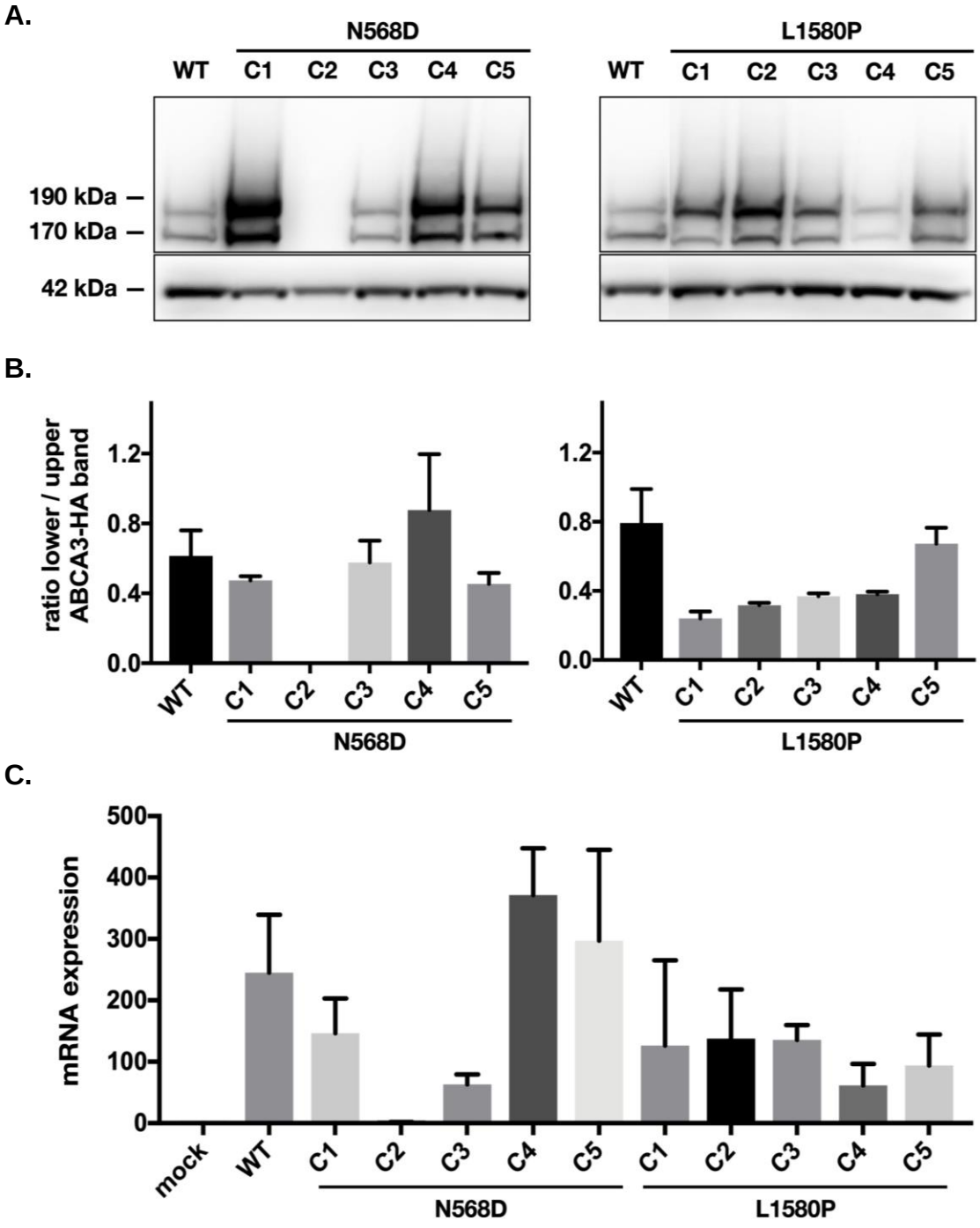

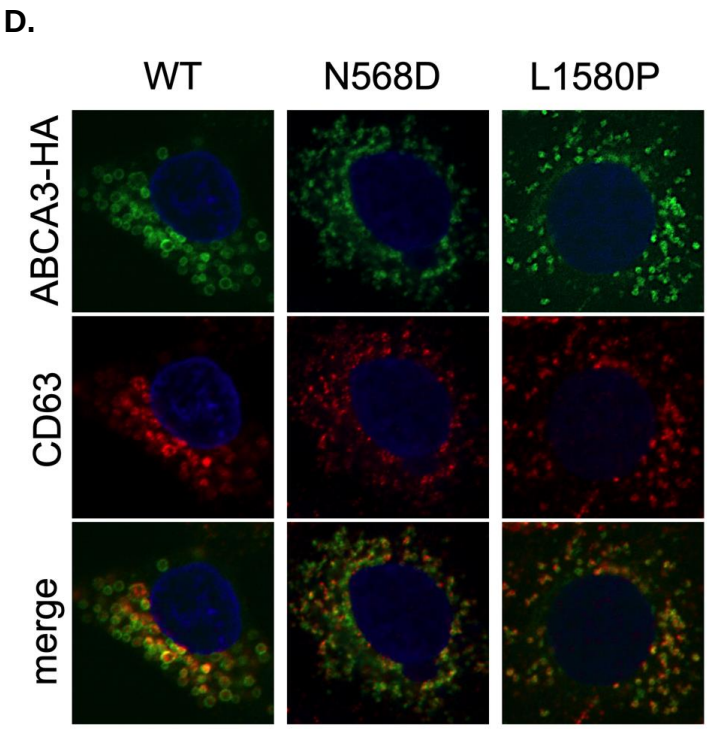

Figure 8. ABCA3-HA stable expressing A549 cells. (**A**) Western blot. For each mutation, 5 clones of single cell colony were cultured and verified the stable expressing of ABCA3-HA by immunoblotting. WT ABCA3-HA has two bands on western blot. ß-actin (42 kDa) was set as reference protein. (**B**) Ratio of lower to upper band intensity on western blot. Images of western blot were analyzed by ImageJ and brightness/contrast was adjusted if necessary. Results of three repeated experiments were showed in bars (mean with SEM). (**C**) mRNA expression level of clones. The mRNA expression of WT and clones of mutation were compared to mock. (**D**) Colocalization of ABCA3-HA with CD63. Similar to WT, The ABCA3+ vesicles of N568D and L1580P were well oval or round-shaped and colocalized with CD63. The figures are cited from Li. Y et al., 2019 and Susanna et al., 2019.

ABCA3-HA have double bands (190 and 170 kDa) on western blot (Fig. 8A). Among all candidates, the ratio of cleaved (lower) to non-cleaved (upper) bands of clone 3 of N568D and clone 5 of L1580P kept the same level as WT (Fig. 8B). Meanwhile, these two clones showed stable mRNA expression in repetitive experiments (Fig. 8C). To certify if the mutated protein reaches LBs, colocalization of ABCA3-HA and CD63, the lysosome marker, was examined by double immunostaining. In confocal, the size of

ABCA3+ vesicles of N568D and L1580P were smaller than WT, while they both showed colocalization with CD63 (Fig. 8D).

5.1.2 Incorporation of propargyl-Cho into phospholipids

No quantification was conducted due to the reference standards for phosphatidyl-propargyl-Cho was not available. Results showed that only WT cells treated with propargyl-Cho contained relevant signals of labeled lipids species as given in Figure 9. For diacyl-phosphatidylcholines, mass transitions were observed in PC.aa.C34.1, PC.aa.C34.2, PC.aa.C32.1, and PC.aa.C32.0 *et al*. (Fig. 9A). The signals of LPC were within the range of blanks and untreated cells, thus incorporation into LPC cannot be

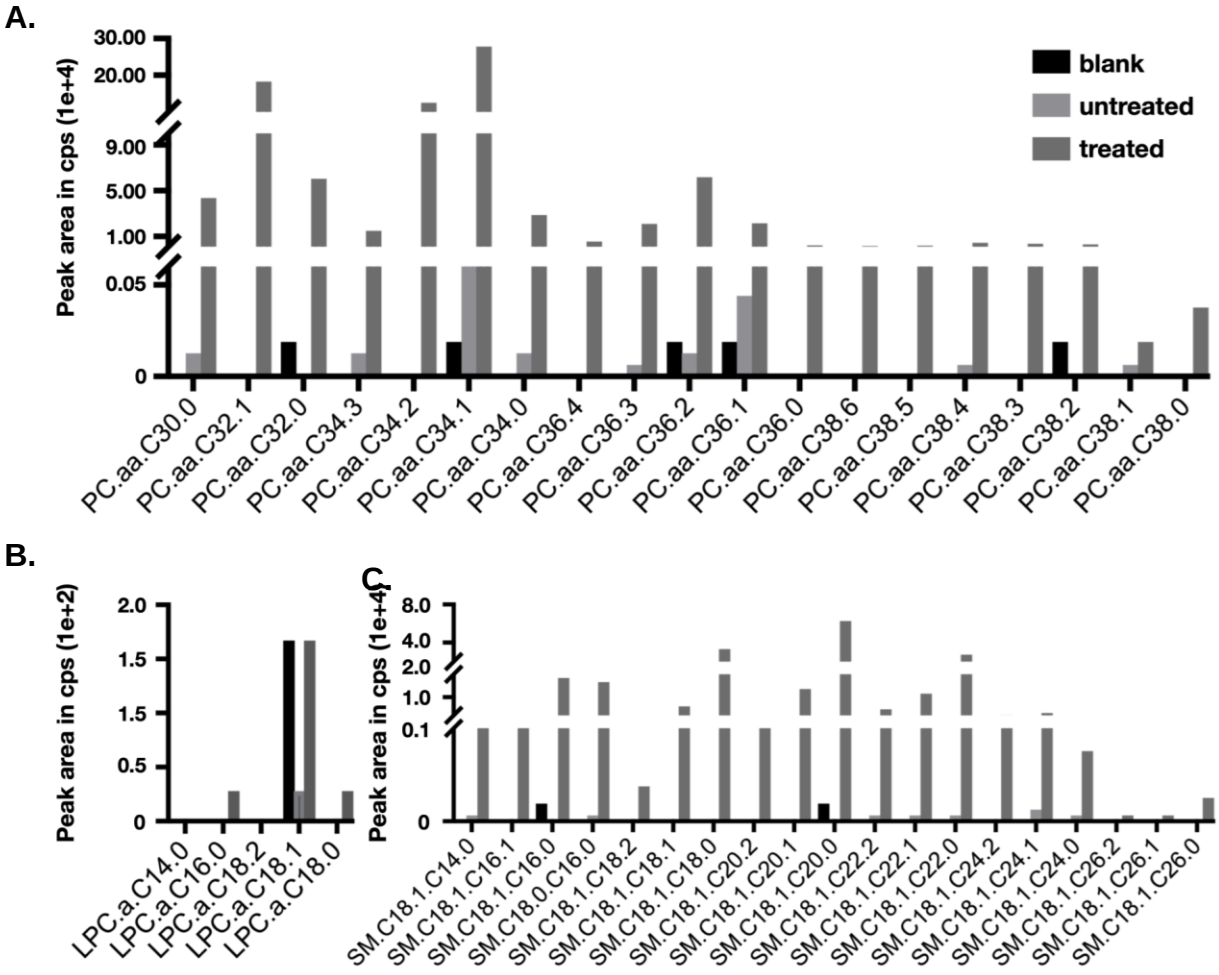

Figure 9. Mean peak areas of propargyl-Cho labeled lipids. (**A**) Phosphatidylcholine labeled with propargyl-Cho. (**B**) Acyl-lyso-phospholipids labeled with propargyl-Cho. (**C**) Sphingomyelins labeled with propargyl-Cho. cps: counts per second.

proven (Fig. 9B). While for another group of choline head phospholipid, subspecies of sphingomyelin were found propargyl-Cho incorporated (Fig. 9C).

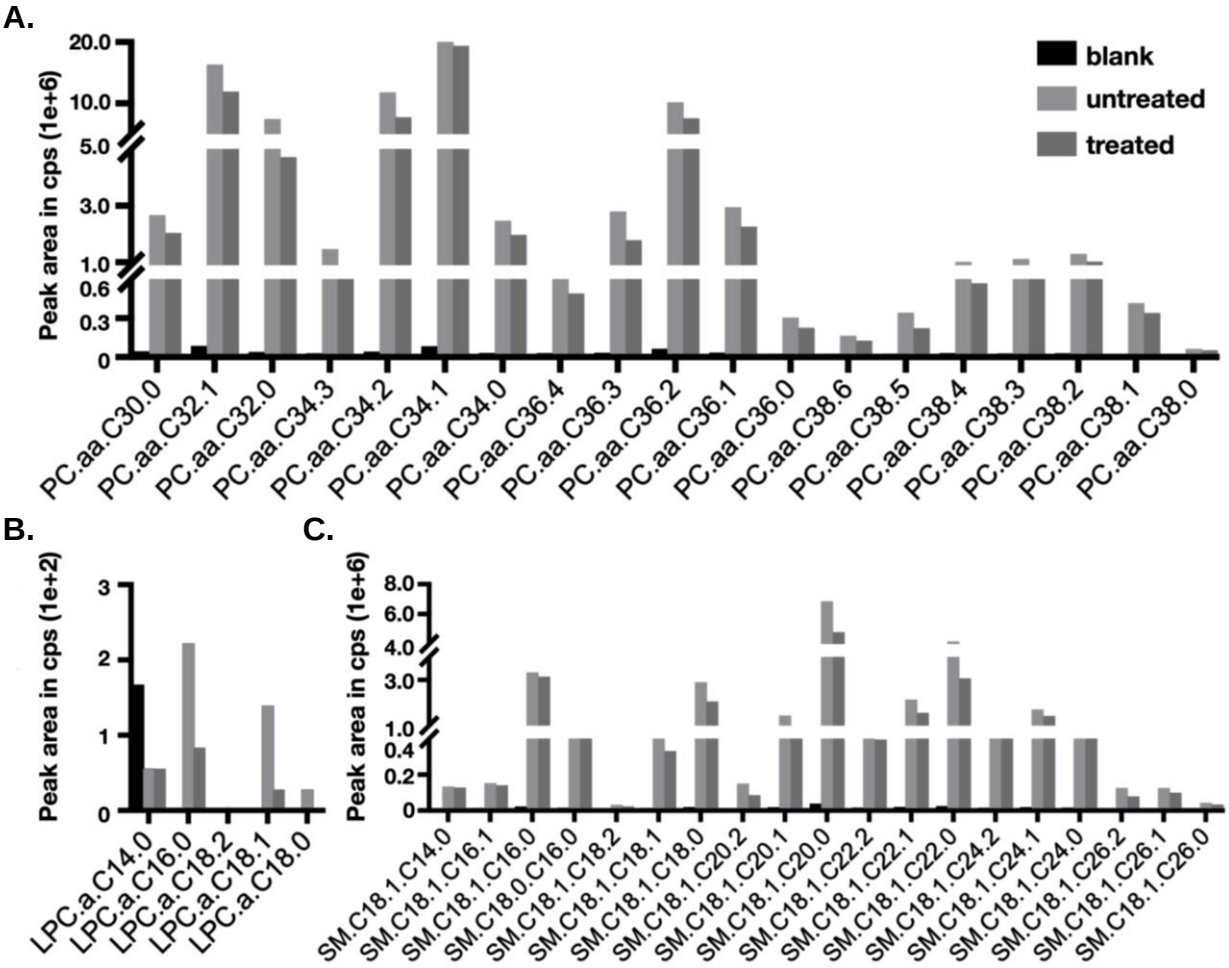

Figure 10. Mean peak areas of choline head lipids. (**A**) Phosphatidylcholine. (**B**) Acyl-lyso-phospholipids (**C**) Sphingomyelins. Choline head lipids were analyzed in WT cells treated with or without propargyl-Cho. The injection and flow rate for different samples were the same.

The results of phosphatidylcholines (Fig. 10) showed that WT cells treated with propargyl-Cho contained slightly less phosphatidylcholines than untreated cells, in both PC and SM group. Signals of LPC were barely detected, but LPC.a.C16.0 and LPC.a.C18.1 in treated cells were less than untreated. In propargyl-Cho treated cells, the mass transition of labeled PC was observed (Fig. 11A), e.g. PC.aa.C32.1, PC.aa.C34.1, and PC.aa.C34.2 et al. Further, cells treated with propargyl-Cho for 24

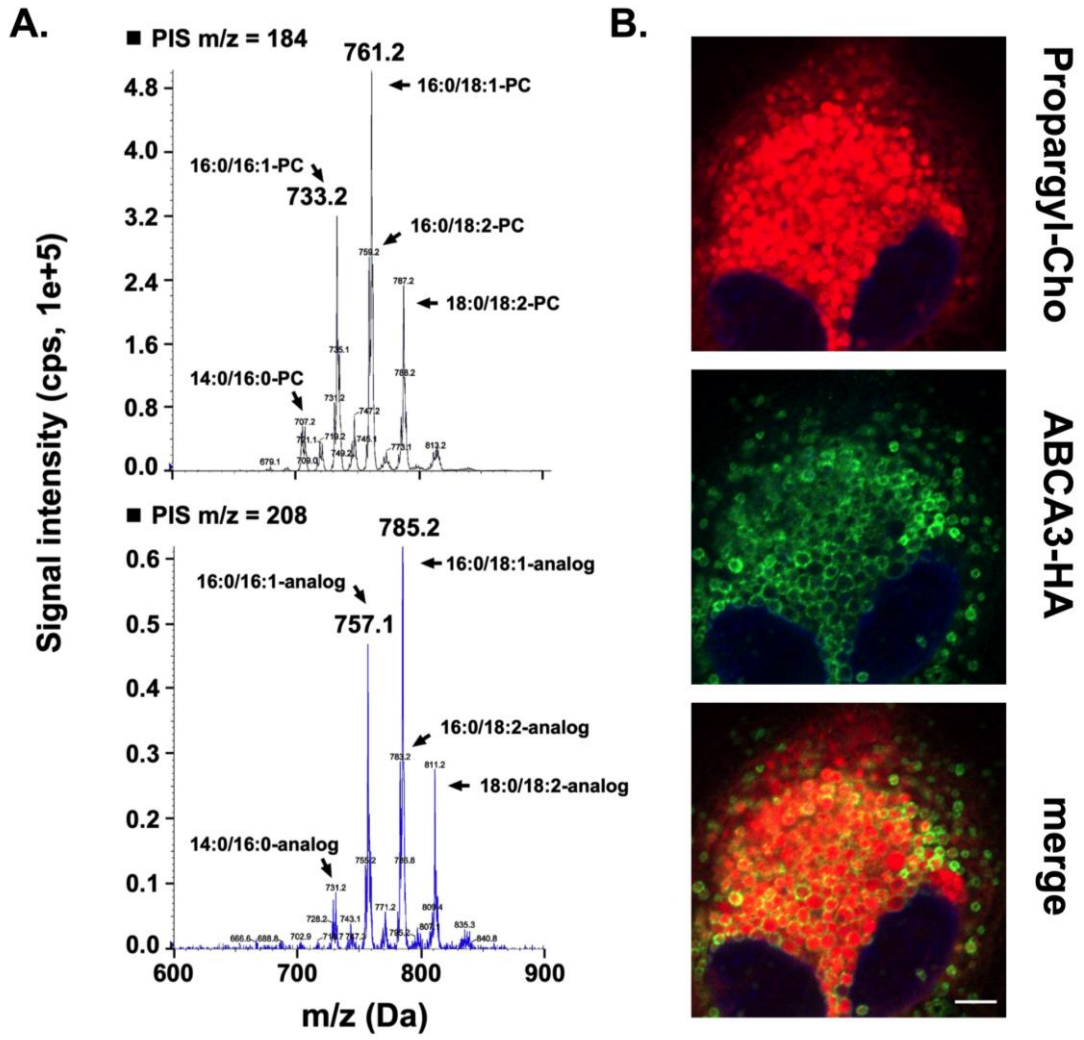

Figure 11. Transfected A549 cells successfully incorporated propargyl-Cho. (**A**) Lipid spectrum. WT cells were treated with (lower panel) or without (upper panel) propargyl-Cho. Upper: phosphatidylcholine. Lower: phosphatidyl-propargyl-Cho. Examples of labeled phosphatidylcholine were marked by arrows. Cps: counts-per-second. PIS: precursor-ion-scan. (**B**) Confocal microscopy. TAMRA-PEG3-Azide marked phosphatidyl-propargyl-Cho by click reaction with the extra alkynyl under Cu (II). Immunostaining of ABCA3-HA protein defined ABCA3+ vesicles. Scale bar: 5μm. The figures are cited from Li. Y et al.

h were conducted with click reaction and visualized with confocal microscopy (Fig. 11B). Fluorescence intensity was uniform inside of ABCA3+ vesicles in focus, meanwhile labeled lipids could be observed outside of vesicles. Lipids signal did not overlay in the nucleus area. These results showed that propargyl-Cho was incorporated by WT cells successfully.

Considering cell bio membranes are mainly composed of choline phospholipids, and that lipids fluorescence signal was observed outside of ABCA3+ vesicles, we examined the colocalization of propargyl-Cho labeled lipids with other membrane structures (Fig. 12). After immunostaining of ER (marker: calnexin), early endosome (marker: EEA1) and Golgi apparatus (marker: GM130), colocalization of phosphatidyl-propargyl-Cho with these membrane structures were observed occasionally (white arrow).

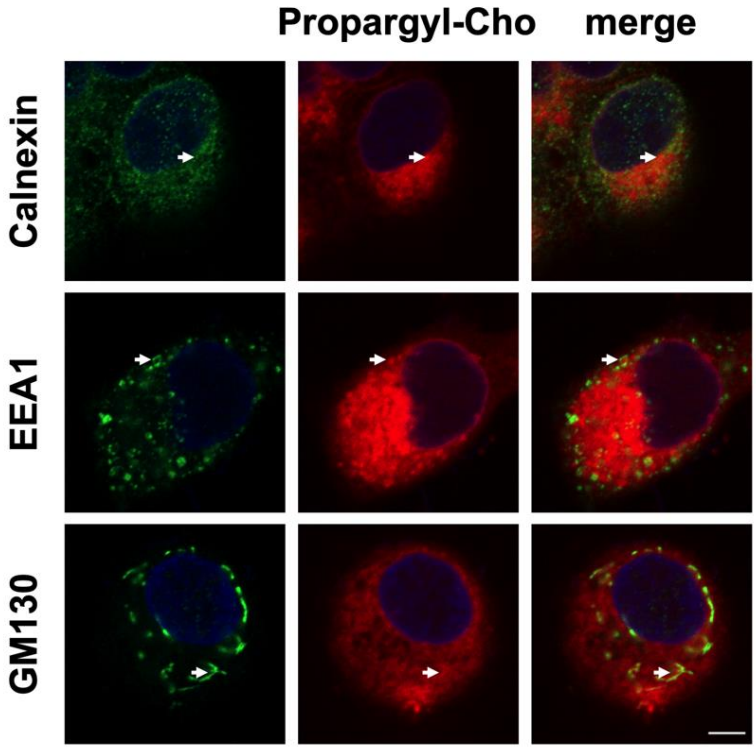

Figure 12. Distribution of propargyl-Cho labeled lipids. Instead of ABCA3-HA, 24 h after pulse-labeling cells were stained with the Calnexin, EEA1 and GM130. Colocalization of referenced sub organelles was marked with white arrows. Scale bar: 5µm. The figures are cited from Li. Y et al.

To ensure the choline analogue is not toxic, WT ABCA3 cells treated with 125 µM propargyl-Cho were monitored cell viability from 4 to 24 h with XTT assay. Compared to untreated cells, the absorbance of treated cells was at the same range at each time point (Fig. 13).

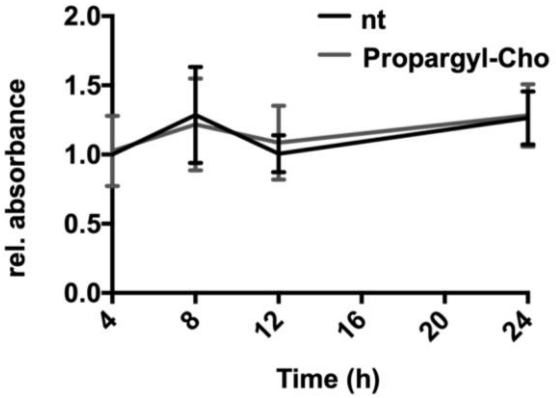

Figure 13. Toxicity of propargyl-Cho. WT cells were seeded in phenol red free RPMI medium supplemented with 10% FCS in 96 well plates and incubated overnight. After pulse-labeling, cells were treated with XTT solution with 100 mM PMS and measured absorbance at 4, 8, 12 and 24 h. Results were from 3 independent experiments. The figures are cited from Li. Y et al.

5.1.3 Incorporation of propargyl-Cho in an ATP dependent manner

To elucidate the incorporation and transportation of propargyl-Cho into our cell model were based on positive consumption of ATP instead of passive diffusion, cells after pulse-labeling were treated with the ATPase inhibitor orthovanadate for 2 h. After inhibition, fluorescence intensity of propargyl-Cho labeled lipids inside of ABCA3+

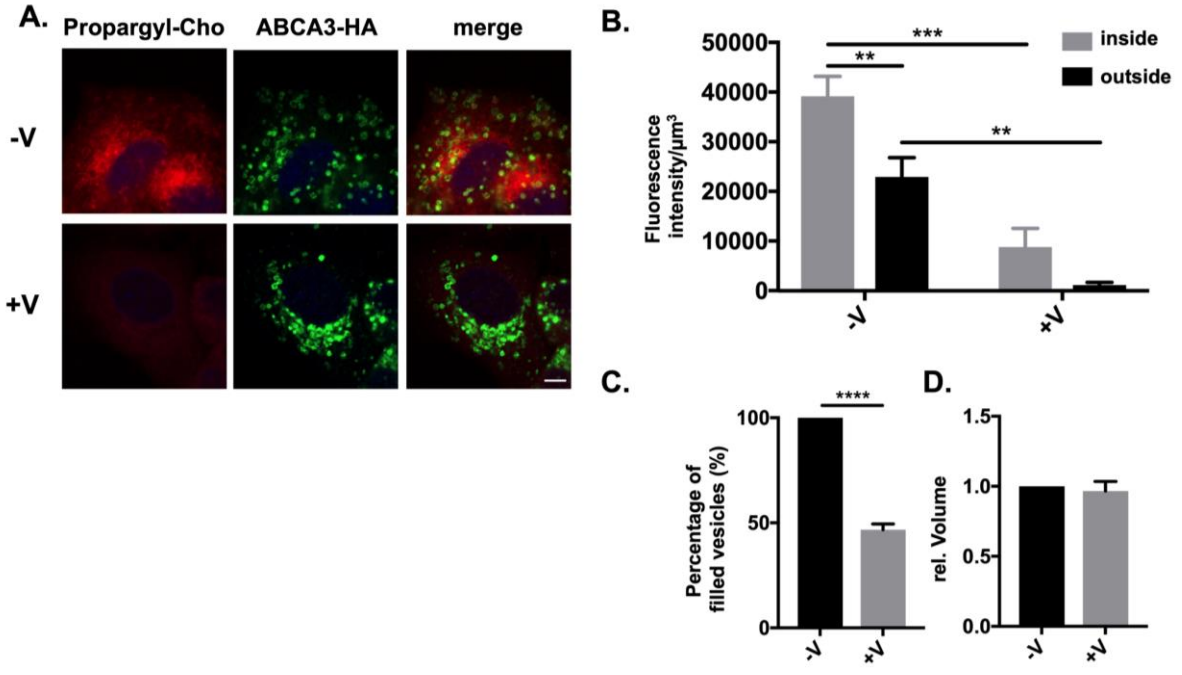

Figure 14. Incorporation of propargyl-Cho in an ATP dependent manner. (**A**) Confocal microscopy of cells with or without inhibition of orthovanadate. -V, without orthovanadate. +V, with orthovanadate. Scale bar: 5 μm. (**B**) Fluorescence intensity inside and outside of vesicles before and after ATPase inhibition. (**C**) The percentage of filled vesicles. (**D**) Relative vesicle volume. Volume of treated cells were compared to untreated. The figures are cited from Li. Y et al.

vesicles reduced to 22.5% of untreated cells, and intensity outside of vesicles decreased to 4.9% (Fig. 14A, B). The percentage of filled vesicles decreased to 46.6% (Fig. 14C). Treatment with orthovanadate did not affect the vesicle volume (Fig. 14D).

5.1.4 Incorporation of propargyl-Cho was concentration dependent

In the concentration dependent experiments about propargyl-Cho incorporation, cells were treated with increasing concentration of propargyl-Cho diluted in OptiMEM, then incubated cells in OptiMEM for another 24 h. Hence the experiment was conducted with the same concentration of choline (which was in OptiMEM). With higher concentration of propargyl-Cho, the fluorescence intensity in ABCA3+ vesicles improved nonlinearly (Fig. 15A, B). When treated with 10 or 250 μM propargyl-Cho, the fluorescence intensity between inside and outside of vesicles were at the same level. While treated with 50 or 125 μM propargyl-Cho, lipids inside vesicles were higher than outside (Fig. 15C). After 24 h, 100% of selected vesicles were filled up with labeled lipids in 125 μM, while only 64% in 50 μM. Therefore 125 μM was set for sequential experiments.

5.1.5 Incorporation of propargyl-Cho was time dependent

Cells in μ-slides were pulse-labeled with 125 μM propargyl-Cho for 30 min then incubated in OptiMEM for distinct time periods. Lipids piled up in ABCA3+ vesicles from 0 to 48 h gradually. Individual ABCA3+ vesicles encompassing massive labeled lipids could be observed since 24 h (Fig. 16A). When observe the time curve of lipids incorporation, the high-speed interval was between 12 to 24 h (Fig. 16B). Conspicuous

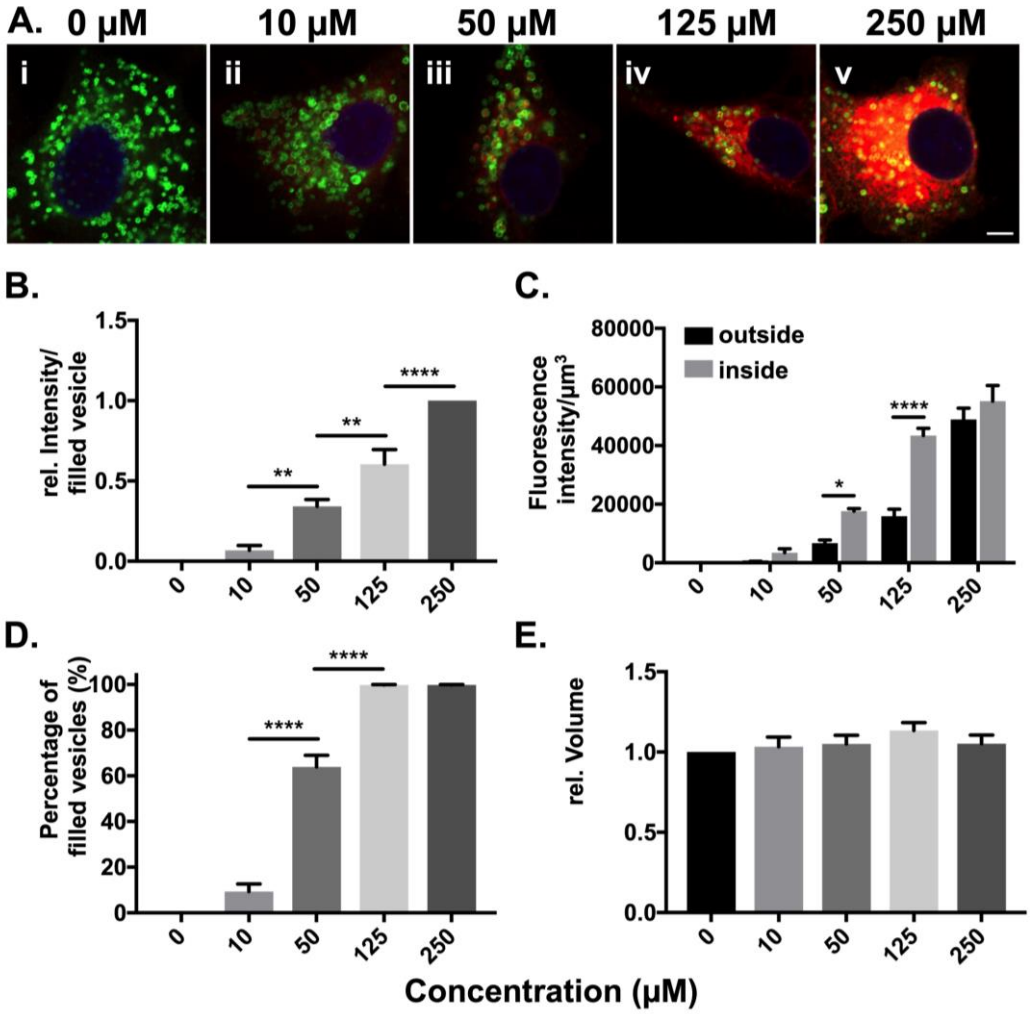

Figure 15. Incorporation of propargyl-Cho was concentration dependent. (**A**) The precondition of the experiment was set as increase concentration of propargyl-Cho while stable concentration for choline. Fluorescence intensity in red channel sharped while the concentration of propargyl-Cho multiplied. Scale bar: 5 µm. (**B**) Lipids intensity inside vesicles relative to the intensity at 250 µM. The lipids intensities were 6.8%, 34.1% and 60.4% of the intensity at 250 µM when treated with 10, 50 and 125 µM respectively. (**C**) Fluorescence outside of vesicles increased in the same trend as inside. Outside of the vesicles, intensities were 38.2% and 36.6% of inside while treated with 50 and 125 µM propargyl-Cho. (**D**) All selected vesicles contained labeled lipids while treated with 125 or 250 µM propargyl-Cho. (**E**) Relative vesicle volume to untreated. *P < 0.0332, **P < 0.0021, **** P < 0.0001. The figures are cited from Li. Y et al.

intensity difference between inside and outside of vesicles appeared after 12 h. At 24 h, fluorescence intensity inside vesicles was nearly 2 folds of that in outside (Fig. 16C).

Approximately 17% of selected vesicles contained propargyl-Cho labeled lipids at 6 h, 57.5% at 12 h and 100% at 24 and 48 h (Fig. 16D).

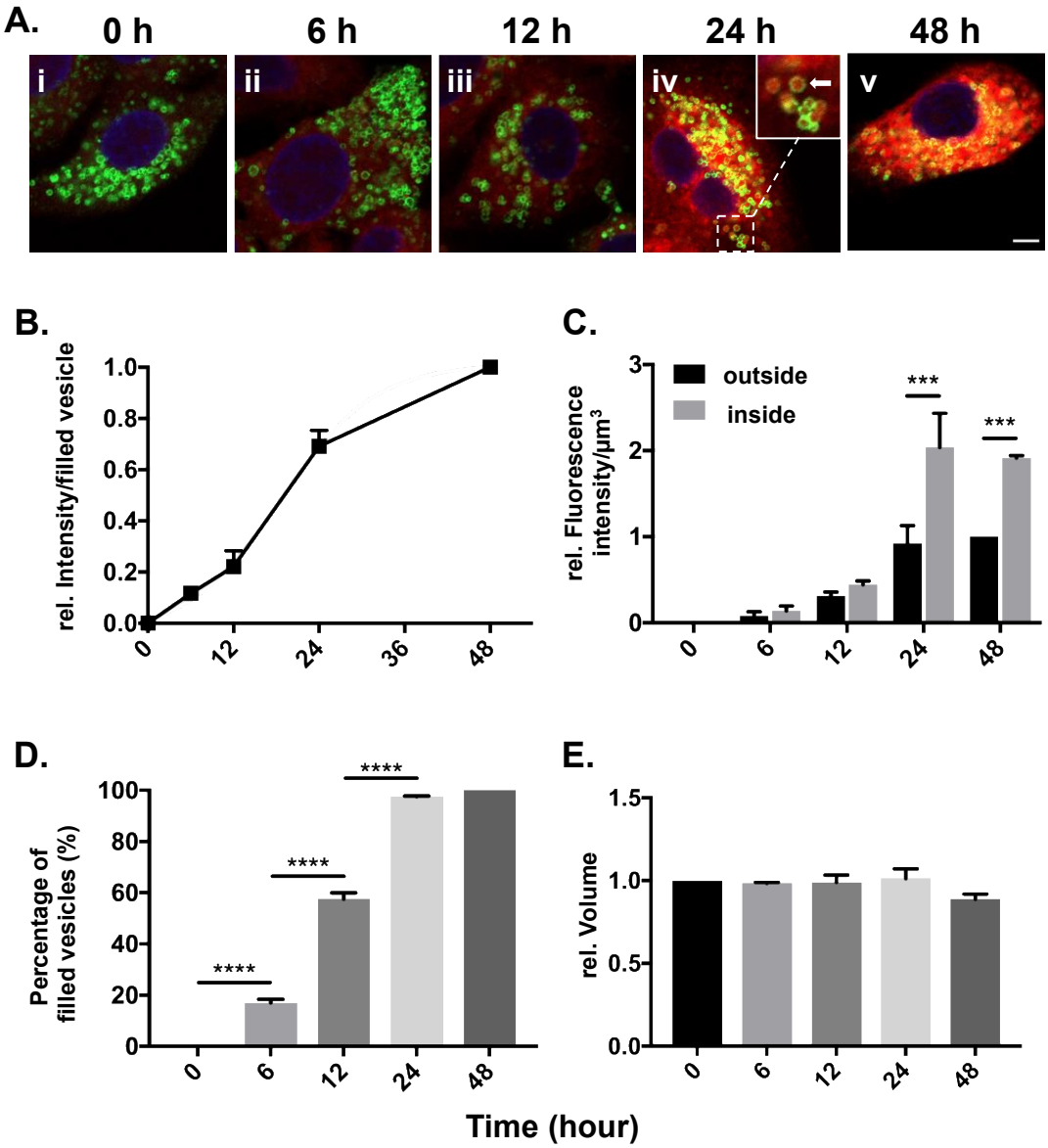

Figure 16. Incorporation of propargyl-Cho was time dependent. (**A**) Confocal images of WT cells treated with 125 µM propargyl-Cho for distinct duration. Massive lipids encompassed in ABCA3+ were arrow marked (iv). Scale bar: 5 µm. (**B**) Time curve of lipids incorporation. Intensities were relative to intensity at 48 h. (**C**) Relative fluorescence intensity/µm^3 inside and outside of vesicles compared to outside intensity at 48 h. Before 24 h, the intensity of in and outside of vesicles were of the same scale. After 24 h, the intensity of outside was only half the amount of intensity inside. (**D**) After 24 h, 100% selected vesicles encompassed labeled lipid. (**E**) Volume of vesicles was steady over time. The figures are cited from Li. Y et al.

5.1.6 Competitive inhibition phosphatidyl-propargyl-Cho transport

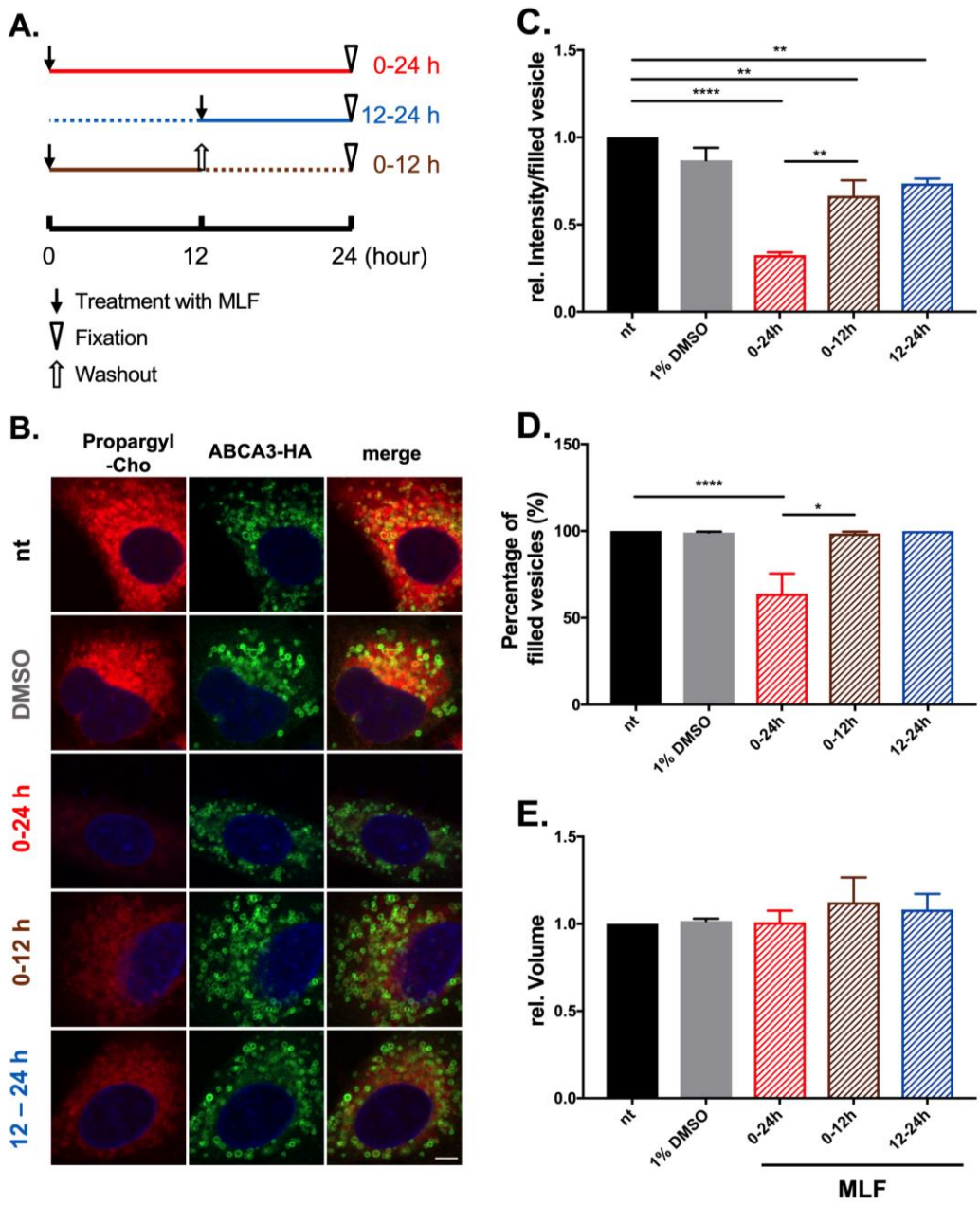

Figure 17. Competitive inhibit phosphatidyl-propargyl-Cho transportation of ABCA3. (**A**) Experiment design for MLF inhibition. The time after pulse-labeling was set as time 0. Cells were incubated for continuous 24 h (0 – 24 h) or washed out after first 12 h (0 – 12 h). Another group of cells were treated with MLF from 12 to 24 h (12 – 24 h). (**B**) Confocal microscopy recording the lipids intensity alteration after MLF treatment. Scale bar: 5 µm. (**C**) Relative fluorescence intensity/μm^3 inside vesicles compared to untreated cells. Either MLF worked on the cells 0 – 24 h, 12 -24 h or 0 – 12h, the lipids intensity reduced compared to untreated. (**D**) MLF on the cells for 24 h reduced the number of vesicles encompassed with propargyl-Cho labeled lipids. (**E**) Volume of vesicles was not affected.

We adopted Miltefosine (MLF), which was reported to be a substrate of ABCA3 in human macrophages [134] to treat WT cells after pulse labeling. Miltefosine was incubated with cells from 0 to 24 h, 12 to 24 h or washed out after 12 h (Fig. 17A). After treatment, the intensity of propargyl labeled lipids decreased in the cells in all circumstances (Fig. 17B). When incubated with MLF in the next 24 h after pulse labeling, the intensity of labeled lipids in the vesicles decreased by 67.5% from nt, and only 63.9% of analyzed vesicles contained labeled lipids. Washing out of MLF after 12 h resumed the filled vesicles percentage to 98.6% and the fluorescence intensity to 73.6% of nt. If MLF inhibition was applied to cells 12 h after labeling, filled percentage was not affected but the intensity in vesicles decreased by 26.6% (Fig. 17C, D). MLF treatment did not influence the cell viability (data did not show) or the vesicle volume (Fig. 17E).

5.1.7 Irreversibly inhibition of phosphocholine synthesis by MN58b

The first reaction in phosphatidyl-propargyl-Cho biosynthesis is catalyzed by choline kinase: ATP delivers a phosphate group to propargyl-Cho and forming phospho-propargyl-Cho. We inhibited the choline kinase of pulse-labeled cells from 0 to 24 h, 0 to 12 h or 12 to 24 h with MN58b, a reported CK inhibitor [6, 135] (Fig. 18A, B). The presence of MN58b on cells from 0 – 24 h reduced labeled lipids in ABCA3+ vesicles by 67.3%. Unlike Miltefosine, washing out of MN58b at 12 h did not enhance the lipids amount inside vesicles (0 – 12 h *vs.* 0 – 24 h). Nevertheless, when the catalytic function of choline kinase was not inhibited in the first 12 h after pulse-labeling, the lipids intensity and filling percentage were not influenced (nt *vs.* 12 – 24 h) (Fig. 18C, D). In each condition, volume of vesicles was not affected by the presence of MN58b.

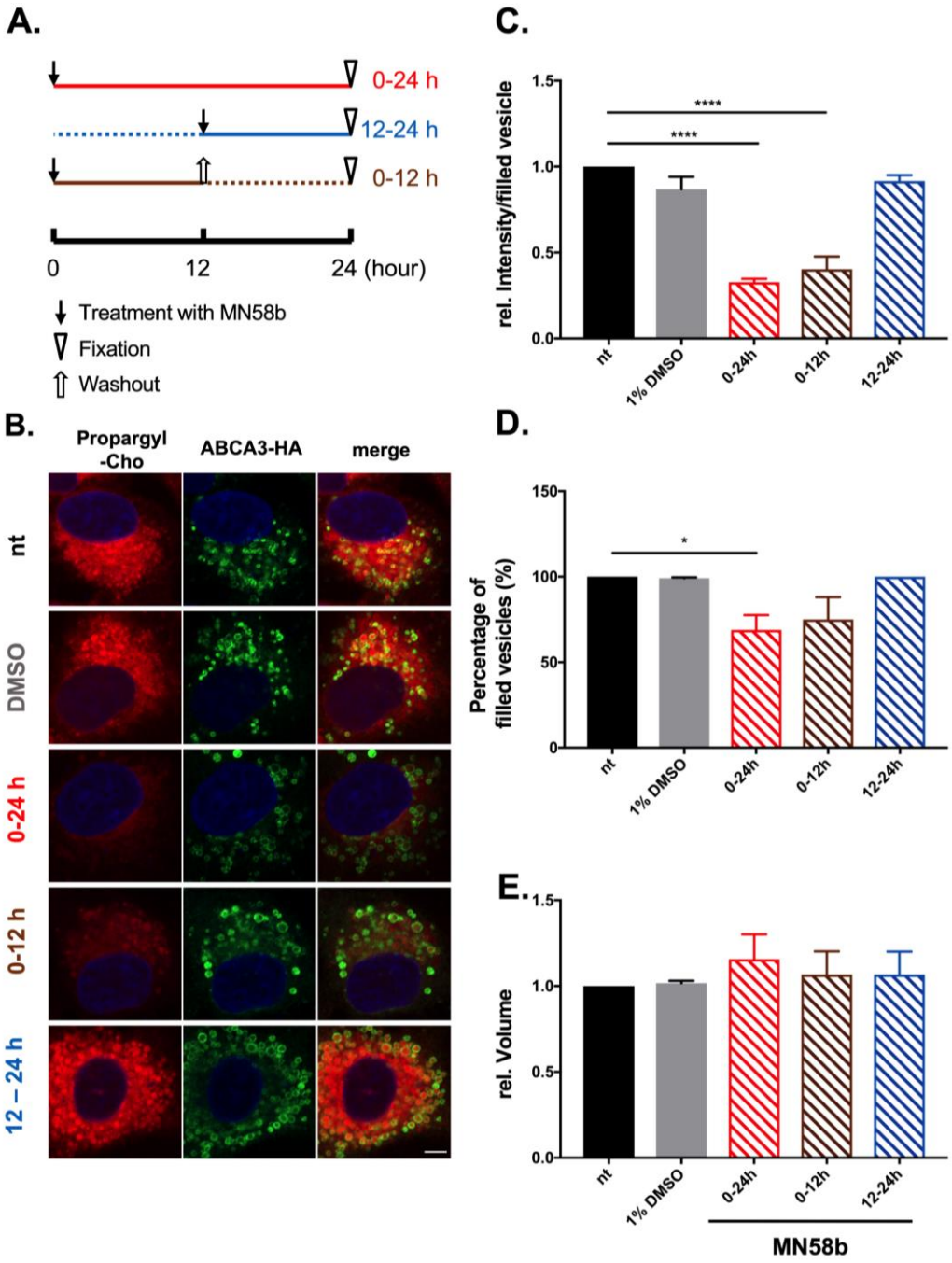

Figure 18. **Irreversibly inhibit the phosphocholine synthesis by MN58b.** (**A**) Experiment design for MN58b inhibition. (**B**) Confocal microscopy of the lipids fluorescence intensity changes after MN58b treatment. Scale bar: 5 μm. (**C**) Relative fluorescence intensity/μm^3 inside vesicles. Compared to untreated cells, treatment with MN58b for 0 – 24 h and 0 – 12 h reduced lipids intensity to 32.7% and 40.3% separately. (**D**) MN58b treatment reduced 31.1% vesicles encompassed with propargyl-Cho labeled lipids (0 – 24 h). (**E**) In each condition, volume of vesicles was not affected by the presence of MN58b.

5.1.8 Deviation of transport function of p.N568D and p.L1580P ABCA3 mutation

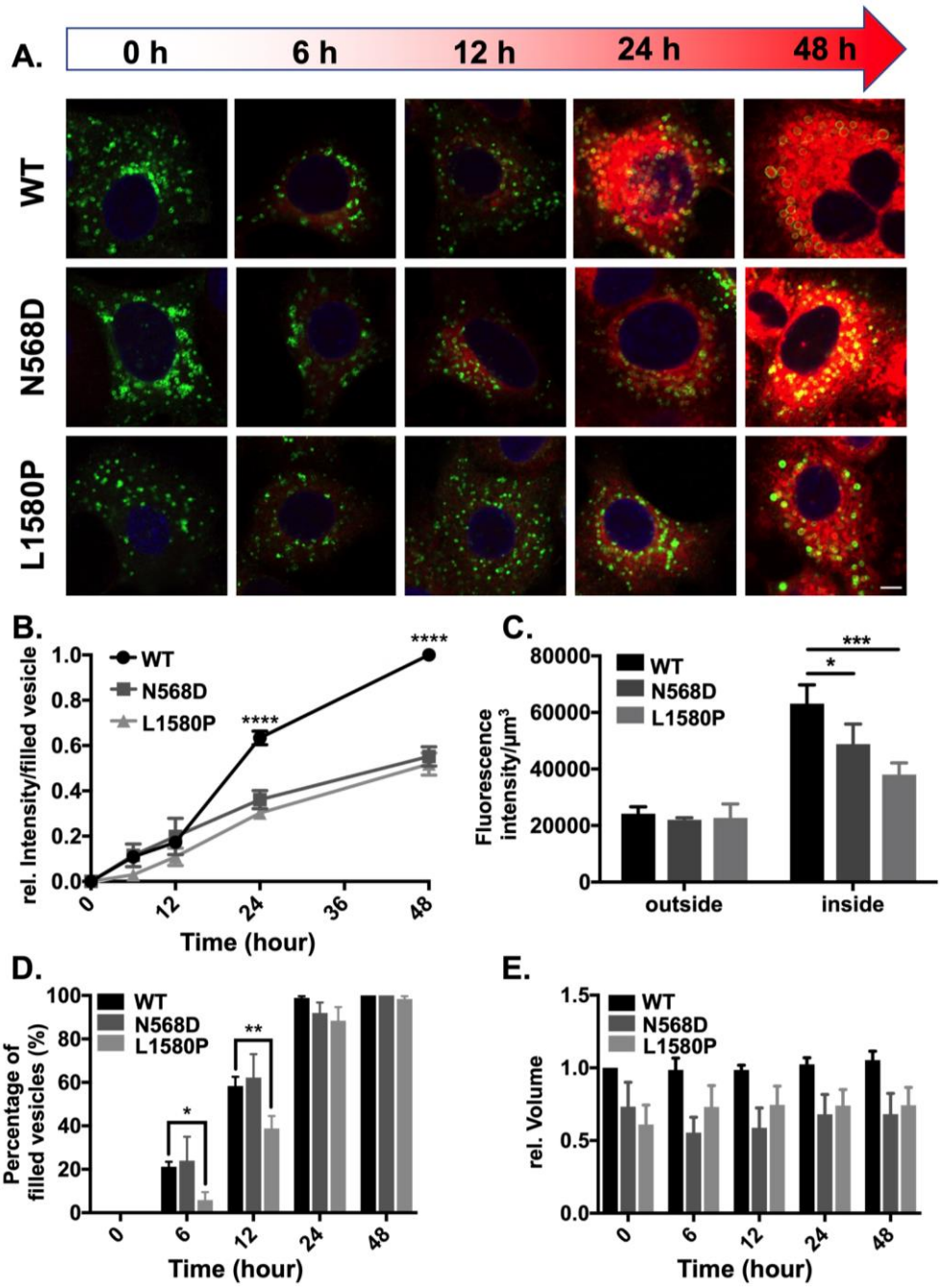

Figure 19. Deviation of transport function of p.N568D and p.L1580P ABCA3 mutation. (**A**) Confocal microscopy of mutants treated with propargyl-Cho and incubated for different time period. Scale bar: 5 μm. (**B**) Propargyl-Cho incorporation time curve of WT and mutants. The ratio was compared to the fluorescence intensity inside WT ABCA3-HA at 48 h. Difference of intensity appeared after 12 h. (**C**) Comparison of the outside and inside intensity among WT and mutants. (**D**) Either in mutations or WT, almost 100% analyzed vesicles contained labeled. (**E**) Mutants vesicle volume were smaller but consistent at each time point. The figures are cited from Li. Y et al.

After we proved that transporting of labeled lipids into vesicles was ABCA3 dependent and that the transport process mainly happened 12 h after pulse-labeling, we tried the method on two patients originated mutations of ABCA3, p.N568D and p.L1580P. Both mutations were reported to undermine ATPase function of ABCA3 [61, 82]. After outlined the time curve of propargyl-Cho labeled lipids incorporation of these two mutations, it showed both the speed and amount of incorporation decreased compared to WT (Fig. 19A, B). Intriguingly, the difference only appeared after 12 h when the transporting process happened. While analyzing the lipids intensity at 24 h, intensity inside p.N568D and p.L1580P ABCA3+ vesicles were 77.4% and 77.8% of WT. However, the intensity outside of vesicles were similar among WT and mutations (Fig. 19C). The vesicle filling percentage of p.L1580P was lower than WT before 24 h but reached 100% at 48 h (Fig. 19D). The vesicle volume of these two mutations were smaller than WT (Fig. 19E).

5.2 Lamellar body isolation

5.2.1 Separation lamellar bodies by sucrose gradient

After 4 h of consecutive ultracentrifuge, successful isolation of lamellar bodies was verified by western blot. While the same amount of protein was added, intensity of ABCA3-HA band in the lane fraction 3 to 5 were higher than other fractions. Condensed

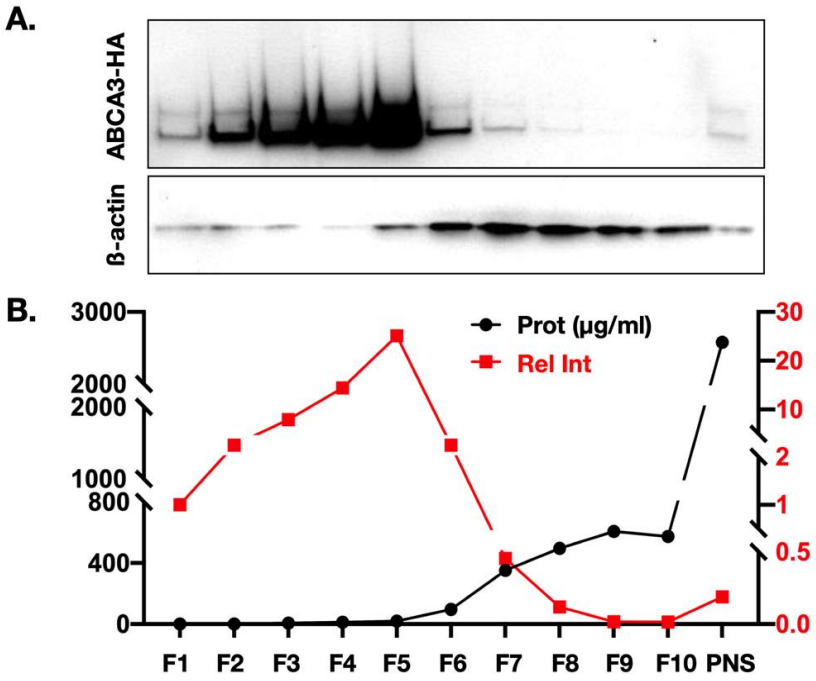

Figure 20. Isolation of lamellar bodies by sucrose gradient. (**A**) For Western blot analysis the same amount of total protein was added. ABCA3-HA and ß-actin was blotted with related antibodies. (**B**) Each fraction was analyzed for protein concentration by Bradford assay. Intensity of ABCA3-HA band was analyzed by ImageJ. Fraction 3 to 5 contained the most abundant ABCA3 protein (red curve) and rather low total protein concentration (black curve) compared to other fractions. The band intensity in all the fractions were compared to fraction 1 (F1).

ABCA3 in F3 to 5 was observed compared to PNS (Fig. 20A, B. Red curve) while the protein concentration in PNS was almost 150 times higher than in F3 to 5 (Fig. 20B, black curve). ß-Actin was reduced in ABCA3 positive fractions.

5.2.2 Intactness of fractionated lamellar bodies

To prove the intactness of isolated lamellar bodies, cells were incubated in 100 nM lysotracker red for 1 h before ultracentrifuge. After fixation and blocking with immunofluorescence buffer without saponin, LTR colocalized well in ABCA3+ vesicles (Fig. 21A, i-iii). While permeabilized of LBs with 1% Triton-X100 or saponin, LTR in ABCA3+ vesicles almost vanished (Fig. 21A, iv, v). In fractions 3 to 5, vesicles around 1 µm diameter size were found LTR positive (Fig 21B).

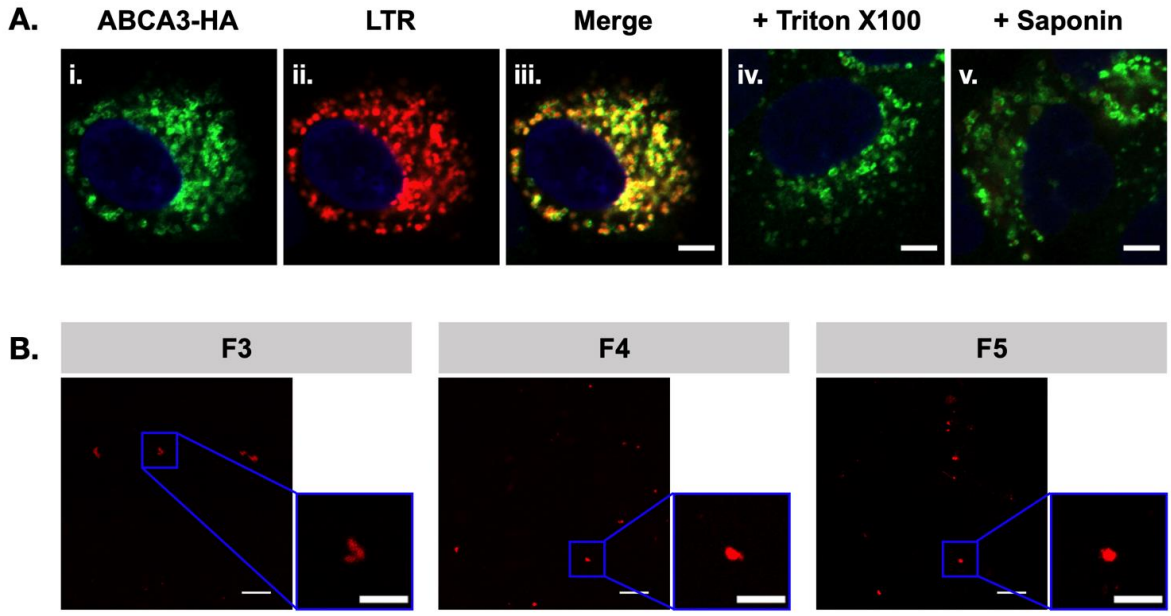

Figure 21. Intactness of fractionated lamellar bodies. (**A**) After incubation with 100 nM LTR for 1 h, ABCA3-HA was stained with HA antibody diluted in immunofluorescence buffer without saponin (i – iii). Fluorescence signal of LTR decreased after permeabilized with 1% Triton-X100 or saponin for 10 min (iv, v). Scale bar: 5 µm. (**B**) After ultracentrifugation, fractions 3 to 5 contained intact lamellar bodies when assessed under confocal microscope. Scale bar in large figures: 10 µm. Scale bar in zoomed in figures: 5 µm.

5.2.3 Purity of fractionated lamellar bodies

To prove the purity of isolated LBs, 16.25 µl of each fraction was mixed with SDS buffer and blotted with marker proteins of other organelles. In F1 to F5, band of ß-Actin was reduced or disappeared. In F7 to F10 and PNS, the marker of early endosome

EEA1 was positive among WT and mutant cells. In post-nuclear supernatant (PNS) mitochondria marker Stoml2 was positive, as in fractions F6 to F10 for L1580P, while in fractions F1 to F5, no contamination of other organelles existed. (Fig. 22).

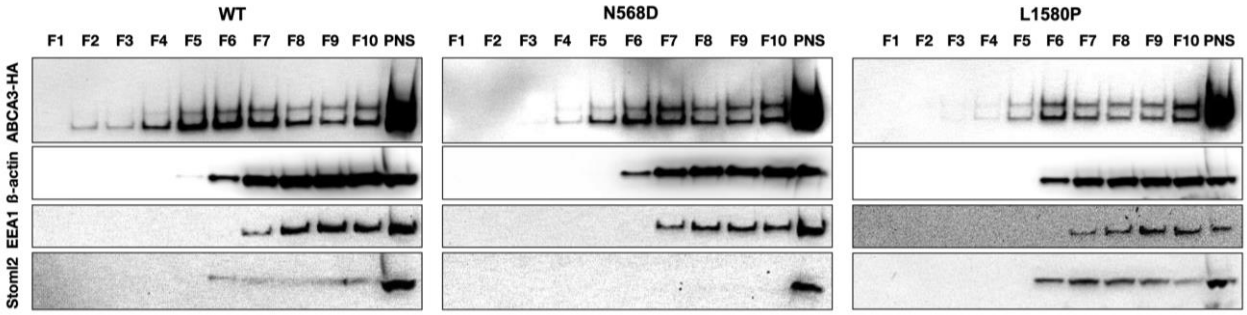

Figure 22. Purity of fractionated lamellar bodies. Western blot of sub organelle markers in fractions of WT, N568D and L1580P. The sample volumes applied to all the lanes were the same. Magnitude of ABCA3-HA signal (LBs) differed between expressed variants. Peak ABCA3-HA expression was in F5-F7, whereas variants N568D and L1580P had fewer signals and peaked in F6, F7 and higher, demonstrating poor separation of LBs from ß-actin and EEA1.

6 Discussion

The present thesis describes a novel approach to study metabolism and trafficking of lipids in cells expressing the ABCA3 transporter, which represents as a new avenue to assess structure-function relationships of this important membrane protein, crucial in the biogenesis of pulmonary surfactant.

We expressed wild type and hypomorphic variants of ABCA3 in A549 epithelial cells, to probe mechanisms for observing transport activity, and rectifying diseased alleles in a cellular setting. To quantify function of ABCA3 alleles, we employed the choline analogue propargyl-Cho. Propargyl-Cho was taken up by A549 cells and converted to the corresponding phospholipid via the enzymes involved in PC synthesis. The resultant phospholipids can be detected using a combination of click chemistry, fluorescence derivatization and microscopy to visualize and quantify the phospholipid end product.

In the study we showed that propargyl-Cho signal was detected in lamellar bodies, endosomes (early and late), and endoplasmic reticulum. At high concentrations it also can be detected in the cytoplasm. The accumulation or detection of labeled phospholipids was ATP-dependent by using ATPase inhibitors. The detection of signal was dependent on choline kinase to incorporate the label into cellular phospholipids. Another substrate of ABCA3 can compete with the transport of propargyl-Cho by ABCA3. Finally, we showed that mutations (p.N568D and p.L1580P) in the ATP-binding cassette of ABCA3 impaired transport function of propargyl-Cho into intracellular vesicles. This method described a new labeled phospholipid that will allow researchers to probe phospholipid handling and transport in more detail.

In the conventional studies of pulmonary biology, the radioactive analogues of choline were most frequently used. Treating isolated alveolar II cells or cell model with [methyl-3H] choline for a certain time period and measure the radioactive intensity or

electron microscopic radioautography unraveled principles of pulmonary PC synthesis. For example, a quantitative time study of feeding choline-deficient mice with [methyl-3H] choline showed that the radioactive PC precursor exclusively accumulated in type II cells when observed with electron microscopy [31]. In ATII cells, [methyl-3H] choline labeled lipids and [3H] leucine label amino acids first appeared in the ER then in Golgi, MVBs and were eventually stored in LBs, indicating the synthesis and traffic routine of lipids and protein of surfactant. This was further verified by Osanai K *et al*. by culturing cells with [methyl-3H] choline or [35S] methionine/cysteine in the presence of the Golgi apparatus disassemble agent, brefeldin A. After lipids extraction, immunoprecipitation and LBs fractionation, it was demonstrated that only surfactant protein transport was a Golgi-dependent act. On the contrary, lipids transport in ATII cells was through a Golgi-independent pathway [32]. Continuing signal decrease of [methyl-3H] choline labeled lipids suggested ongoing secretion and turnover of LBs [136]. In 1975, scientists found in cortisol treated human fetal lung tissue that the intensity of [methyl-3H] choline labeled phosphatidylcholine increased with the number of lamellar bodies, which suggested that in early ages cortisol could increase the surfactant production [137].

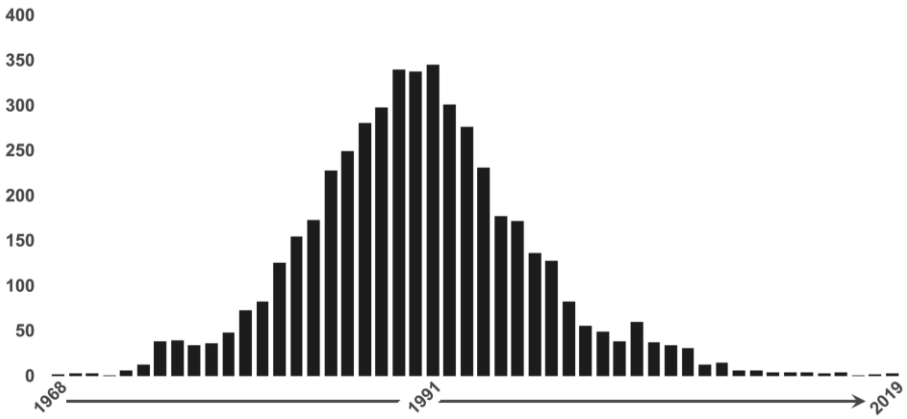

Figure 23. Literatures with '[^{3}H] choline' in PubMed. By searching for the key word '[^{3}H]' choline in PubMed, we found the number of literatures contained in this field increased yearly from 1968 to 1991, then decreased gradually to only 1 or 2 literatures per year. Data was from NCBI.

However, with the emerging appearance of new non-radioactive choline analogues and tough barriers to entry radioactive experiments around the world (Fig. 23), researchers turned to employ more environment-friendly analogues. Among commercially available fluorescence PC analogues, one category is 7-nitro-2-1,3-benzoxadiazol-4-yl (NBD) labeled lipids such as NBD-PC, PE, PS, SM, ceramide and cholesterol. Although the NBD-lipids were only discovered a few decades ago, they are the first choice to study the biology of membrane [138]. For example, C6-NBD-PC was extensively utilized in studying the dynamics of DPPC bilayer [139, 140]. In the study of Weichert N *et al*., C_{12}-NBD-PC and C_{12}-NBD-PE were observed to colocalize with WT ABCA3+ vesicles under confocal microscope, but not with p.R43L, p.L101P and p.R280C mutated ABCA3 [141]. However, the number of colocalization of NBD lipids with ABCA3 was few, not to mention to understand the dynamic, or quantity of ABCA3 transport function.

Another fluorescence analogue of lipids is BODIPY labeled phospholipid. In microalgae, BODIPY 505/515 was a rapid, practical and non-expensive choice for neutral lipids staining [142-144]. To study the removal of DPPC/dioleoyl phosphatidylcholine (DOPC) from mineral surface by microphages, Das AR *et al*. used BODIPY labeled DPPC* to coat quartz or kaolin particles and realized the removal of DPPC* or DOPC was independent of the mineral specific characteristics [145]. Other studies chose BODIPY stained SP-B protein rather than lipids to elucidate the biogenesis or function of surfactant [146-148]. Thus, to understand the phospholipids transport function of ABCA3, neither NBD nor BODIPY labeled lipids are good choices.

In 2009, Jao CY *et al*. synthesized a choline analogue named propargyl-choline to metabolic label choline containing phospholipids in cultured cells and animals [130]. Unlike radioactive choline analogue or NBD-/BODIPY- lipids, propargyl-Cho is a non-radioactive and rather small analogue that supposed to participate in the biogenesis

pathway of choline. In NIH 3T3 cells, after 24 h culture and click reaction with Alexa568-azide, propargyl-Cho was found to be efficiently and intensely incorporated into Cho group phospholipids. Either in plasma membrane or intracellular structures, the staining of propargyl-Cho could be visualized. There were no signs of cellular toxicity when the concentration of propargyl-Cho reached as high as 500 μM. With electrospray ionization-tandem mass spectrometry (ESI-MS/MS) assay, propargyl-Cho was found to incorporate efficiently into all Cho head phospholipids. The ratio of labeled Cho was in accordance with the increasing concentration of propargyl-Cho. 18% and 33% of Cho was replaced by propargyl-Cho when labeled with 100 and 250 μM propargyl-Cho separately. Thus, this method provided a clear and convenient way to study the biology of choline and choline phospholipids *in vitro* and *in vivo*.

Propargyl-Cho – azide fluorophore click reaction method described Jao CY *et al*. was then applied in various studies. Luo Z and collogues established an optical imaging method to monitor the choline change when cancer cells were treated with a chemotherapy reagent, cisplatin [149]. In the study, click reaction of propargyl-Cho happened with Alexa-488 azide. The fluorescence of labeled Cho phospholipids decreased as the concentration of cisplatin increased. Luo Z *et al.* then applied this method on isolated head and neck cancer biopsies and found the intensity of labeled lipids was observed to be 4 or 5 fold higher compared to control tissues [150], which provided an alternative pathological diagnosis method for physicians. Propargyl-Cho was also used in another lipid enriched cells – neuro system to assess the myelin remyelination in animal multiple sclerosis model [129]. In the central neural system of the tested animal model, newly synthesized myelin could be visualized and quantified through propargyl-Cho labeling. With this method, the authors found glatiramer acetate could promote the remyelination in experimental autoimmune encephalomyelitis. Beside in mammalian cells, propargyl-Cho was also used in plants and *Streptococcus*

pneumoniae to clarify the biological characteristics of choline phospholipids in these species [151, 152].

In the present study, the behavior of propargyl-Cho shared similarities with the aforementioned studies. Successful incorporation of propargyl-Cho into ABCA3 expressing A549 cells was confirmed by both confocal microscopy and lipids mass spectrometry. Same as the results from Jao CY *et al*., three species of choline head phospholipids, phosphatidylcholine, lysophosphatidylcholine and sphingomyelin were labeled with propargyl as shown by mass spectrometry. Similarly, the concentration dependent incorporation of the analogue was non-linear. This is in accordance with our observation of a 5-fold increase of propargyl-Cho concentration only resulted in 2.9-fold increase of fluorescence intensity in ABCA3+ vesicles (250 µM vs. 50 µM).

With long exposure time, the fluorescence signal of propargyl-Cho in cells treated with a high concentration (1 mM) could be detected 30 min after treatment, while under short camera exposure, the time course was 3 to 6 h [130]. In our study, the fluorescent labeled lipids could be observed 6 h after pulse labeling, the signal kept stably increasing until 48 h, which conform to those experiments conducted with radioactive [^{3}H] choline, indicating a similar behavior of propargyl-Cho in A549 cells to natural choline [153, 154].

To investigate whether propargyl-Cho transporting across the plasmatic membrane and among sub organelles occurred in an ATP dependent active transfer or a passive transfer manner, we inhibited the ATPase of cells by sodium orthovanadate (NO_3VO_4). NO_3VO_4 is a common ATPase inhibitor utilized to study the function of ABC transporters [155-157]. In this study, after NO_3VO_4 treatment the amount of lipids decreased both in and outside of ABCA3+ vesicles, suggesting the transport of propargyl-Cho was an ATP dependent active but not passive transfer.

To eliminate the interference of background lipids intensity, which was unavoidable since phospholipids was necessary components of bio membranes, we took several conductions. First, we verified the colocalization of propargyl-Cho labeled lipids with other intracellular structures such as ER and early endosomes. Then, during each independent confocal microscopy, the pinhole, laser power, digital gain and offset for each image and Z-stack were set properly to avoid noise and high background. With all the measures set already as above the fluorescence signal outside of ABCA3+ vesicles were still visible. Therefore, we analyzed the intensity outside of vesicles to help interpreting the results.

In the time dependent experiments intensity of labeled lipids outside of vesicles increased synchronously with the intensity inside, however, the disparity between in and outside only appeared after 12 h. 12 h was also a watershed that the lipids intensity inside WT ABCA3+ vesicles was higher in mutant ABCA3+ vesicles after but not before. In A549 cells and ATII cells from rat, the incorporation of [methyl-3H] choline into PC could be observed as soon as 60 min after labeling [158]. In the study of Voelker DR *et al*., the saturated DPPC in the LB fraction increased gradually in the first 8 h after chasing with radioactive choline for 20 min [159]. While the desaturated PC activity in LBs increased steadily in the first 12 h after administration of [methyl-3H] choline [160]. It is plausible that the synthesis of propargyl-PC in the vesicles mainly happened from initial point to 12 h.

To ascertain this speculation, we chose two time points (0 and 12 h) to expose cells to MN58b. Without interfering the function of other enzymes of *De novo* synthesis pathway such as CTT, CHPT or PAP, MN58b specifically targets choline kinase and decreases the synthesis of phosphatidylcholine [135]. Exposure to MN58b supposed to significantly decrease the uptake of choline at certain dose, causing ER stress and triggering apoptosis of cancer cells [6, 135, 161-163]. The working concentration of

MN58b in A549 cells was 10 μM, which exhibited no cell toxicity and inhibited PC synthesize irreversibly. Intriguingly, the inhibition only worked when cells were exposed to MN58b for the first 12 h (either washed out or not), but not after 12 h. Thus, it is proved that the PC accumulated in LBs in 24 h was mainly synthesized in the first 12 h, which was in accordance with the results from [^{3}H] choline labeling experiments [158-160].

In the study of visceral and cutaneous leishmaniasis, Dolmen LC *et al*. found that when infected human macrophages exposed to Miltefosine (hexadecyl phosphocholine), an alkylated phosphatidylcholine as the only licensed oral medical treatment for the parasite, ABCA3 transporter expression on cell membrane was highly induced. During the antileishmanial process, the role of ABCA3 was to impede the treatment by transport MLF out of macrophages, while knockdown of ABCA3 by shRNA reduced leishmanial survival [134]. The authors concluded that ABCA3 on the membrane of macrophages act as MLF efflux transporter. As a predict competitor of propargyl-Cho labeled PC transported by ABCA3, MLF treatment decreased the labeled lipids in LBs in the present study. The inhibition was partially released after washing out of MLF at 12 h.

However, interpretation of the results in MLF inhibition should be rather careful. In a Langmuir monolayer model mimicking natural cell membrane, MLF interacted strongly with cholesterol in the monolayer rather that phosphatidylcholine [164]. And in HepG2 cells MLF hampered cholesterol trafficking to ER and reduced the synthesis of PC [165]. By comparing the [^{3}H] choline uptake in control and MLF treated cells, Geilen C *et al*. proposed that the translocation of choline phosphate cytidyltransferase (CHPT) was inhibited by the phosphocholine analogue [166]. The influence of MLF on the phospholipid's membrane stability and lipids homeostasis thence cannot be ignored.

Combining the results from MN58b and MLF inhibition experiments, we recognized that the fluorescence intensity of labeled lipids inside ABCA3+ vesicles at 24 h was an index of specific ABCA3 choline-head phospholipids transport function. To further confirm the guess and make the propargyl-Cho assay applicable, we described the same time curve of propargyl-Cho incorporation curve from two reported functional mutations of ABCA3, p.N568D and p.1580P. cDNA variate from A to G at 1702 site in ABCA3 lead the missense mutation of p.N568D, which was first found in a patient (compound heterozygous) who died after lung transplantation and described by Shulenin S *et al* [93]. In the same study, p.L1580P (c. 4739T>C) was identified in a patient (homozygous) who died in the neonatal period of life. The asparagine inside Walker A motif mutated to aspartic acid, disturbing the conserved structure of nucleotide binding domain 1 of ABCA3. Although L1580P just 'located close to NBD2', side-chain size change and potential helix break contribute to the impaired ATP hydrolysis. Other mutations in the transmembrane domain (T1114M, G1221S) of ABCA3 may cause aberrant function of the protein although the exact mechanism was not clear [61, 87]. Matsumara Y et, al. found the ATP binding capacity of N568D and L1580P decreased to 60% and 54% of WT, which resulted in an ATP hydrolysis by N568D and L1580P was 12 and 9% of that of WT protein. Vanadate-induced nucleotide trapping partially explained the loss of NBDs function of ABCA3, but the direct impact of the variants' influence on the phospholipids transport function was not measured. In our study, the phosphatidyl-propargyl-Cho transport function of these two mutations were quantified. Compared to WT ABCA3, the total amount lipids accumulated in LBs of p.N568D and p.L1580P ABCA3 decreased dramatically, indicating the loss of transport function of these mutations. These results suggested that propargyl-Cho assay is a practical tool to characterize the function of newly identified ABCA3 mutation and to assist find new treatment strategy of related disease.

The phospholipids transport function of p.N568D and p.L1580P were also characterized in a previous study by TopF-PC assay with a similar analyzing strategy [87]. The results of TopF-PC assay showed that the transport activity of p.N568D and p.L1580P decreased to 14% and 10% of WT separately, while propargyl-Cho assay showed the reduction of transport function were 77% and 78% of WT. There was a study indicating that in rat ATII cells the uptake of [^{3}H] choline labeled natural surfactant was much higher than synthetic phospholipids liposomes, and the difference increased with culturing time [167]. Thus, the distinguished transport function measured by TopF-PC (synthetic phospholipids liposomes) and propargyl-Cho (natural surfactant) could be explained. The short comes of TopF-PC were discussed in part 1.1.5 and in our published paper [168]. Except for the difference associated with the theory of the label into the cell system, there were many similarities between these two methods: incorporation of these two reagents was time, concentration and ATP dependent transportation. Considering that up to date propargyl-Cho assay is limited usage on fixed cells only, while TopFluor lipids are utilized in live cell imaging [169-171], we expected that the combination of these two methods will together open the possibility of additional insights into the biogenesis and transport of surfactant lipids.

We characterized a new functional assay of ABCA3 utilizing propargyl-Cho, and in previous studies we found correctors and potentiators that were potential treatments for ChILD patients [87, 114, 168]. Despite phosphatidylcholine, lipids such as cholesterol and phosphatidylglycerol may also play important roles in surfactant biology. Novel methods to measure the transport function of other lipids of ABCA3 await to be established. In this effort, we tried to isolate LBs in WT ABCA3 expressing A549 cells for further lipidomic analysis. With the classical sucrose gradient fractionation method [172-174], we isolated LBs successfully. Lamellar bodies distributed mainly in fractions 3 to 5 with high purity. Isolated LBs from p.N568D and

p.L1580P also existed in fraction 5. LBs are now prepared for lipidomic analysis. Due to the complexity, massive labor and materials requirement of sucrose gradient isolation, combining specialties of LBs and fluorescence activated flowcytometry sorting of sub organelles might help to isolate LBs efficiently [175-177].

Although applying propargyl-Cho to isolated type II cells would definitely benefit the study, we do not have a source for isolated human ATII cells. Regarding that the genotype of A549 cells and primary ATII cells are different from each other, an altered model could be human induced pluripotent stem (IPS) cells with and without mutations. Another problem related to primary cell is the lack of availability of ABCA3 antibodies which can reliably label this protein in the ATII cells. Although the use of A549 cells as an ATII cell model has several limitation [178, 179], lamellar bodies like structures were expressed by transfection with ABCA3 [83, 131]. Recently, it was reported that air-liquid interface (ALI) culturing of A549 cells induced a more ATII cell-like phenotype, such as SP-C expression and thyroid transcription factor-1, and the morphology analysis showed A549 cells reconstituted epithelial layers in ALI [180, 181]. ALI culturing could be a choice to study the function of secretion of surfactant lipids by LBs in ATII cells in the future.

In conclusion, we applied an interesting method to interrogate ABCA3-dependent lipid transport in living cells. We expressed wild type and mutants of ABCA3 in A549 epithelial cells, to probe mechanisms for phospholipids transport activity with a choline analogue followed by click reaction for visualization. In general, A549 cells do not closely resemble alveolar type II cells, but their application in this study provided a facile method to study ABCA3 related functions.

7 Publication

1. Li, Y., S. Kinting, S. Hoppner, M. E. Forstner, O. Uhl, B. Koletzko and M. Griese (2019). "Metabolic labelling of choline phospholipids probes ABCA3 transport in lamellar bodies." Biochim Biophys Acta Mol Cell Biol Lipids 1864(12): 158516.
2. Kinting, S., Y. Li, M. Forstner, F. Delhommel, M. Sattler and M. Griese (2019). "Potentiation of ABCA3 lipid transport function by ivacaftor and genistein." J Cell Mol Med 23(8): 5225-5234.

8 AFFIDAVIT/ EIDESSTATTLICHE VERSICHERUNG

Hiermit versichere ich an Eides statt, dass ich die vorliegende Dissertation „ Probe the transport function of ABCA3 by metabolic labelling of choline phospholipids “ selbstständig angefertigt habe, mich außer der angegebenen keiner weiteren Hilfsmittel bedient und alle Erkenntnisse, die aus dem Schrifttum ganz oder annähernd übernommen sind, als solche kenntlich gemacht und nach ihrer Herkunft unter Bezeichnung der Fundstelle einzeln nachgewiesen habe.

I hereby confirm that the dissertation “Probe the transport function of ABCA3 by metabolic labelling of choline phospholipids" is the result of my own work and that I have only used sources or materials listed and specified in the dissertation.

Li, Yang 29.09.2020, Munich

9 Acknowledgements

This thesis has been greatly influenced by the guidance and support of a number of people. First of all, none of this work would have been possible without Prof. Matthias Griese, who provided me with unyielding scientific and professional support and mentorship over the last four years. Looking back, I am amazed at all I have learned from his advising throughout my doctorate study which supports my development as an independent scientist.

The process of finishing my doctorate study involved a great deal of time spent in lab with some wonderful colleagues. I am very appreciative of the friendship, partnership and generous support that were always there from Dr. Susanna Kinting, who lead me though the ‘early’ years in the lab. And I am very grateful for the unconditional support and help from Dr. Forstner, Luise, Steffi, Christina, Traudl, and Frau Schams. Together with Lisa, Pippa and Xiaohua, I spent the most wonderful and happy time in my journey. I am so fortunate that I worked in such a lovely group.

I want to express my gratitude to Dr. Olaf Uhl for his wonderful job in mass spectrometry study and valuable advices. I would also like to thank our collaborators from other laboratories for their most valuable help in my work.

My family have always provided a grounded base for me, and I am forever grateful for their love, support and encouragement over the last four years. A lot thanks to my best friend Xuemei, the most beautiful and talent woman in the world who always shares happiness with me.

Finally, I thank Min, the man I love and respect deeply. His love has always been a truly invaluable component to this work and my life.

10 Reference

1. v. Neergaard, K., *Neue Auffassungen über einen Grundbegriff der Atemmechanik.* Zeitschrift für die gesamte experimentelle Medizin, 1929. **66**(1): p. 373-394.
2. Avery, M.E. and J. Mead, *Surface properties in relation to atelectasis and hyaline membrane disease.* AMA J Dis Child, 1959. **97**(5, Part 1): p. 517-23.
3. Engle, W.A., F. American Academy of Pediatrics Committee on, and Newborn, *Surfactant-replacement therapy for respiratory distress in the preterm and term neonate.* Pediatrics, 2008. **121**(2): p. 419-32.
4. Pinkerton, K.E., *et al*., *Morphologic changes in the lung during the lifespan of Fischer 344 rats.* Am J Anat, 1982. **164**(2): p. 155-74.
5. Ramos, B., *et al*., *Inhibition of CTP:phosphocholine cytidylyltransferase by C(2)-ceramide and its relationship to apoptosis.* Mol Pharmacol, 2002. **62**(5): p. 1068-75.
6. Al-Saffar, N.M., *et al*., *Noninvasive magnetic resonance spectroscopic pharmacodynamic markers of the choline kinase inhibitor MN58b in human carcinoma models.* Cancer Res, 2006. **66**(1): p. 427-34.
7. Gault, C.R., L.M. Obeid, and Y.A. Hannun, *An overview of sphingolipid metabolism: from synthesis to breakdown.* Adv Exp Med Biol, 2010. **688**: p. 1-23.
8. Batenburg, J.J., *Surfactant phospholipids: synthesis and storage.* Am J Physiol, 1992. **262**(4 Pt 1): p. L367-85.
9. Hallman, M., B.L. Epstein, and L. Gluck, *Analysis of labeling and clearance of lung surfactant phospholipids in rabbit. Evidence of bidirectional surfactant flux between lamellar bodies and alveolar lavage.* J Clin Invest, 1981. **68**(3): p. 742-51.
10. Geiger, K., M.L. Gallagher, and J. Hedley-Whyte, *Cellular distribution and clearance of aerosolized dipalmitoyl lecithin.* J Appl Physiol, 1975. **39**(5): p. 759-66.
11. Wright, J.R., *Clearance and recycling of pulmonary surfactant.* Am J Physiol, 1990. **259**(2 Pt 1): p. L1-12.
12. Jacobs, H., *et al*., *The significance of reutilization of surfactant phosphatidylcholine.* J Biol Chem, 1983. **258**(7): p. 4159-65.
13. Jobe, A.H., *et al*., *Surfactant phosphatidylcholine metabolism and surfactant function in preterm, ventilated lambs.* Am Rev Respir Dis, 1989. **139**(2): p. 352-9.
14. Oyarzun, M.J., J.A. Clements, and A. Baritussio, *Ventilation enhances pulmonary alveolar clearance of radioactive dipalmitoyl phosphatidylcholine in liposomes.* Am Rev Respir Dis, 1980. **121**(4): p. 709-21.
15. Mason, R.J. and M.C. Williams, *Phospholipid composition and ultrastructure of A549 cells and other cultured pulmonary epithelial cells of presumed type II cell origin.* Biochim Biophys Acta, 1980. **617**(1): p. 36-50.
16. Veldhuizen, R., *et al*., *The role of lipids in pulmonary surfactant.* Biochim Biophys Acta, 1998. **1408**(2-3): p. 90-108.
17. Griese, M., *et al*., *Quantitative Lipidomics in Pulmonary Alveolar Proteinosis.* Am J Respir Crit Care Med, 2019. **200**(7): p. 881-887.
18. Agassandian, M. and R.K. Mallampalli, *Surfactant phospholipid metabolism.* Biochim Biophys Acta, 2013. **1831**(3): p. 612-25.
19. Johansson, J. and T. Curstedt, *Molecular structures and interactions of pulmonary surfactant components.* Eur J Biochem, 1997. **244**(3): p. 675-93.

20. Casals, C., *Role of surfactant protein A (SP-A)/lipid interactions for SP-A functions in the lung.* Pediatr Pathol Mol Med, 2001. **20**(4): p. 249-68.
21. Whitsett, J.A. and T.E. Weaver, *Hydrophobic surfactant proteins in lung function and disease.* N Engl J Med, 2002. **347**(26): p. 2141-8.
22. Hawgood, S., *Surfactant: composition, structure, and metabolism.*, in *In The Lung: Scientific Foundations, 2nd Ed.* 1997, Lippincott-Raven Publishers, Philadelphia. p. PA. 557–571.
23. Goerke, J., *Pulmonary surfactant: functions and molecular composition.* Biochim Biophys Acta, 1998. **1408**(2-3): p. 79-89.
24. Wang, Z., S.B. Hall, and R.H. Notter, *Roles of different hydrophobic constituents in the adsorption of pulmonary surfactant.* J Lipid Res, 1996. **37**(4): p. 790-8.
25. Yukitake, K., *et al*., *Surfactant apoprotein A modifies the inhibitory effect of plasma proteins on surfactant activity in vivo.* Pediatr Res, 1995. **37**(1): p. 21-5.
26. Crouch, E. and J.R. Wright, *Surfactant proteins a and d and pulmonary host defense.* Annu Rev Physiol, 2001. **63**: p. 521-54.
27. Shepherd, V.L., *Distinct roles for lung collectins in pulmonary host defense.* Am J Respir Cell Mol Biol, 2002. **26**(3): p. 257-60.
28. Mavis, R.D., J.N. Finkelstein, and B.P. Hall, *Pulmonary surfactant synthesis. A highly active microsomal phosphatidate phosphohydrolase in the lung.* J Lipid Res, 1978. **19**(4): p. 467-77.
29. Jobe, A., *et al*., *Characterization of phospholipids and localization of some phospholipid synthetic and subcellular marker enzymes in subcellular fractions from rabbit lung.* Biochim Biophys Acta, 1981. **666**(1): p. 47-57.
30. Magoon, M.W., *et al*., *Subfractionation of lung surfactant. Implications for metabolism and surface activity.* Biochim Biophys Acta, 1983. **750**(1): p. 18-31.
31. Chevalier, G. and A.J. Collet, *In vivo incorporation of choline- 3 H, leucine- 3 H and galactose- 3 H in alveolar type II pneumocytes in relation to surfactant synthesis. A quantitative radoautographic study in mouse by electron microscopy.* Anat Rec, 1972. **174**(3): p. 289-310.
32. Osanai, K., *et al*., *Pulmonary surfactant transport in alveolar type II cells.* Respirology, 2006. **11 Suppl**: p. S70-3.
33. Osanai, K., R.J. Mason, and D.R. Voelker, *Pulmonary surfactant phosphatidylcholine transport bypasses the brefeldin A sensitive compartment of alveolar type II cells.* Biochim Biophys Acta, 2001. **1531**(3): p. 222-9.
34. Voelker, D.R., *New perspectives on the regulation of intermembrane glycerophospholipid traffic.* J Lipid Res, 2003. **44**(3): p. 441-9.
35. Toulmay, A. and W.A. Prinz, *Lipid transfer and signaling at organelle contact sites: the tip of the iceberg.* Curr Opin Cell Biol, 2011. **23**(4): p. 458-63.
36. Perez-Gil, J. and T.E. Weaver, *Pulmonary surfactant pathophysiology: current models and open questions.* Physiology (Bethesda), 2010. **25**(3): p. 132-41.
37. Wustner, D., *et al*., *Vesicular and nonvesicular transport of phosphatidylcholine in polarized HepG2 cells.* Traffic, 2001. **2**(4): p. 277-96.

38. Lin, S., *et al*., *Lysophosphatidylcholine Acyltransferase 1 (LPCAT1) Specifically Interacts with Phospholipid Transfer Protein StarD10 to Facilitate Surfactant Phospholipid Trafficking in Alveolar Type II Cells.* J Biol Chem, 2015. **290**(30): p. 18559-74.
39. Chander, A., *et al*., *Lung lamellar bodies maintain an acidic internal pH.* J Biol Chem, 1986. **261**(13): p. 6126-31.
40. Woodworth, B.A., *et al*., *Presence of surfactant lamellar bodies in normal and diseased sinus mucosa.* ORL J Otorhinolaryngol Relat Spec, 2005. **67**(4): p. 199-202.
41. Toyoshima, K. and B. Tandler, *Dense-cored vesicles and unusual lamellar bodies in type III gustatory cells in taste buds of rabbit foliate papillae.* Acta Anat (Basel), 1989. **135**(4): p. 365-9.
42. Svane-Knudsen, V., G. Rasmussen, and P.P. Clausen, *Surfactant-like lamellar bodies in the mucosa of the human nose.* Acta Otolaryngol, 1990. **109**(3-4): p. 307-13.
43. Martensson, J., *et al*., *Glutathione metabolism in the lung: inhibition of its synthesis leads to lamellar body and mitochondrial defects.* Proc Natl Acad Sci U S A, 1989. **86**(14): p. 5296-300.
44. Holland, V.F., G.A. Zampighi, and S.A. Simon, *Morphology of fungiform papillae in canine lingual epithelium: location of intercellular junctions in the epithelium.* J Comp Neurol, 1989. **279**(1): p. 13-27.
45. Hills, B.A., *Oesophageal surfactant: evidence for a possible mucosal barrier on oesophageal epithelium.* Aust N Z J Med, 1994. **24**(1): p. 41-6.
46. Hills, B.A., *Gastric mucosal barrier: evidence for Helicobacter pylori ingesting gastric surfactant and deriving protection from it.* Gut, 1993. **34**(5): p. 588-93.
47. Bouwstra, J., *Structure of the skin barrier and its modulation by vesicular formulations.* . Progress in Lipid Research, 2003. **42(1), 1–36.**
48. Elias, P.M., & Friend, D. S, *The permeability barrier in mammalian epidermis.* The Journal of Cell Biology, 1975. **65(1), 180–191**.
49. Griese, M., *et al*., *Surfactant lipidomics in healthy children and childhood interstitial lung disease.* PLoS One, 2015. **10**(2): p. e0117985.
50. Thannhauser, S.J., J. Penotti, and N.F. Boncoddo, *Isolation and properties of hydrolecithin (dipalmityl lecithin) from lung; its occurrence in the sphingomyelin fraction of animal tissues.* J Biol Chem, 1946. **166**(2): p. 669-75.
51. Hayashi, H., *et al*., *Molecular species profiles of acidic phospholipids in lung fractions of adult and perinatal rabbits.* Biochim Biophys Acta, 1990. **1042**(1): p. 126-31.
52. Adachi, H., *et al*., *Characterization of phospholipids accumulated in pulmonary-surfactant compartments of rats intratracheally exposed to silica.* Biochem J, 1989. **262**(3): p. 781-6.
53. Kahn, M.C., *et al*., *Phosphatidylcholine molecular species of calf lung surfactant.* Am J Physiol, 1995. **269**(5 Pt 1): p. L567-73.
54. Meban, C., *Effect of lipids and other substances on the adsorption of dipalmitoyl phosphatidylcholine.* Pediatr Res, 1981. **15**(7): p. 1029-31.
55. Zen, K., *et al*., *Generation and characterization of monoclonal antibodies to alveolar type II cell lamellar body membrane.* Am J Physiol, 1998. **275**(1): p. L172-83.
56. Mulugeta, S., *et al*., *Identification of LBM180, a lamellar body limiting membrane protein of alveolar type II cells, as the ABC transporter protein ABCA3.* J Biol Chem, 2002. **277**(25): p. 22147-55.

57. Besnard, V., *et al*., *Conditional deletion of Abca3 in alveolar type II cells alters surfactant homeostasis in newborn and adult mice.* Am J Physiol Lung Cell Mol Physiol, 2010. **298**(5): p. L646-59.
58. Bruder, E., *et al*., *Ultrastructural and molecular analysis in fatal neonatal interstitial pneumonia caused by a novel ABCA3 mutation.* Mod Pathol, 2007. **20**(10): p. 1009-18.
59. Cheong, N., *et al*., *ABCA3 is critical for lamellar body biogenesis in vivo.* J Biol Chem, 2007. **282**(33): p. 23811-7.
60. Garmany, T.H., *et al*., *Surfactant composition and function in patients with ABCA3 mutations.* Pediatr Res, 2006. **59**(6): p. 801-5.
61. Matsumura, Y., *et al*., *Characterization and classification of ATP-binding cassette transporter ABCA3 mutants in fatal surfactant deficiency.* J Biol Chem, 2006. **281**(45): p. 34503-14.
62. Theodoulou, F.L. and I.D. Kerr, *ABC transporter research: going strong 40 years on.* Biochem Soc Trans, 2015. **43**(5): p. 1033-40.
63. Kos, V. and R.C. Ford, *The ATP-binding cassette family: a structural perspective.* Cell Mol Life Sci, 2009. **66**(19): p. 3111-26.
64. Dean, M., Y. Hamon, and G. Chimini, *The human ATP-binding cassette (ABC) transporter superfamily.* J Lipid Res, 2001. **42**(7): p. 1007-17.
65. Borst, P. and R.O. Elferink, *Mammalian ABC transporters in health and disease.* Annu Rev Biochem, 2002. **71**: p. 537-92.
66. Hyde, S.C., *et al*., *Structural model of ATP-binding proteins associated with cystic fibrosis, multidrug resistance and bacterial transport.* Nature, 1990. **346**(6282): p. 362-5.
67. Ban, N., *et al*., *ABCA3 as a lipid transporter in pulmonary surfactant biogenesis.* J Biol Chem, 2007. **282**(13): p. 9628-34.
68. Yamano, G., *et al*., *ABCA3 is a lamellar body membrane protein in human lung alveolar type II cells.* FEBS Lett, 2001. **508**(2): p. 221-5.
69. Weng, J., *et al*., *Insights into the function of Rim protein in photoreceptors and etiology of Stargardt's disease from the phenotype in abcr knockout mice.* Cell, 1999. **98**(1): p. 13-23.
70. Valverde, M.A., *et al*., *Volume-regulated chloride channels associated with the human multidrug-resistance P-glycoprotein.* Nature, 1992. **355**(6363): p. 830-3.
71. Nies, A.T. and D. Keppler, *The apical conjugate efflux pump ABCC2 (MRP2).* Pflugers Arch, 2007. **453**(5): p. 643-59.
72. Cheong, N., *et al*., *Functional and trafficking defects in ATP binding cassette A3 mutants associated with respiratory distress syndrome.* J Biol Chem, 2006. **281**(14): p. 9791-800.
73. Allikmets, R., *A photoreceptor cell-specific ATP-binding transporter gene (ABCR) is mutated in recessive Stargardt macular dystrophy.* Nat Genet, 1997. **17**(1): p. 122.
74. Rust, S., *et al*., *Tangier disease is caused by mutations in the gene encoding ATP-binding cassette transporter 1.* Nat Genet, 1999. **22**(4): p. 352-5.
75. Bodzioch, M., *et al*., *The gene encoding ATP-binding cassette transporter 1 is mutated in Tangier disease.* Nat Genet, 1999. **22**(4): p. 347-51.
76. Doan, M.L., *et al*., *Clinical, radiological and pathological features of ABCA3 mutations in children.* Thorax, 2008. **63**(4): p. 366-73.

77. Stahlman, M.T., *et al*., *Expression of ABCA3 in developing lung and other tissues.* J Histochem Cytochem, 2007. **55**(1): p. 71-83.
78. Nagata, K., *et al*., *Human ABCA3, a product of a responsible gene for abca3 for fatal surfactant deficiency in newborns, exhibits unique ATP hydrolysis activity and generates intracellular multilamellar vesicles.* Biochem Biophys Res Commun, 2004. **324**(1): p. 262-8.
79. Hofmann, N., *et al*., *Analysis of the Proteolytic Processing of ABCA3: Identification of Cleavage Site and Involved Proteases.* PLoS One, 2016. **11**(3): p. e0152594.
80. Frixel, S., *et al*., *Homooligomerization of ABCA3 and its functional significance.* Int J Mol Med, 2016. **38**(2): p. 558-66.
81. Beers, M.F., *et al*., *Disruption of N-linked glycosylation promotes proteasomal degradation of the human ATP-binding cassette transporter ABCA3.* Am J Physiol Lung Cell Mol Physiol, 2013. **305**(12): p. L970-80.
82. Matsumura, Y., *et al*., *ABCA3-mediated choline-phospholipids uptake into intracellular vesicles in A549 cells.* FEBS Lett, 2007. **581**(17): p. 3139-44.
83. Wittmann, T., *et al*., *Tools to explore ABCA3 mutations causing interstitial lung disease.* Pediatr Pulmonol, 2016. **51**(12): p. 1284-1294.
84. Engelbrecht, S., *et al*., *The surfactant lipid transporter ABCA3 is N-terminally cleaved inside LAMP3-positive vesicles.* FEBS Lett, 2010. **584**(20): p. 4306-12.
85. Park, S.K., *et al*., *Identification and characterization of a novel ABCA3 mutation.* Physiol Genomics, 2010. **40**(2): p. 94-9.
86. Paolini, A., *et al*., *Structural Features of the ATP-Binding Cassette (ABC) Transporter ABCA3.* Int J Mol Sci, 2015. **16**(8): p. 19631-44.
87. Kinting, S., *et al*., *Potentiation of ABCA3 lipid transport function by ivacaftor and genistein.* J Cell Mol Med, 2019. **23**(8): p. 5225-5234.
88. Zhou, Y., P. Ojeda-May, and J. Pu, *H-loop histidine catalyzes ATP hydrolysis in the E. coli ABC-transporter HlyB.* Phys Chem Chem Phys, 2013. **15**(38): p. 15811-5.
89. Hopfner, K.P., *et al*., *Structural biology of Rad50 ATPase: ATP-driven conformational control in DNA double-strand break repair and the ABC-ATPase superfamily.* Cell, 2000. **101**(7): p. 789-800.
90. De la Rosa, M.B. and S.W. Nelson, *An interaction between the Walker A and D-loop motifs is critical to ATP hydrolysis and cooperativity in bacteriophage T4 Rad50.* J Biol Chem, 2011. **286**(29): p. 26258-66.
91. Fitzgerald, M.L., *et al*., *ABCA3 inactivation in mice causes respiratory failure, loss of pulmonary surfactant, and depletion of lung phosphatidylglycerol.* J Lipid Res, 2007. **48**(3): p. 621-32.
92. Hammel, M., *et al*., *Targeted inactivation of the murine Abca3 gene leads to respiratory failure in newborns with defective lamellar bodies.* Biochem Biophys Res Commun, 2007. **359**(4): p. 947-51.
93. Shulenin, S., *et al*., *ABCA3 gene mutations in newborns with fatal surfactant deficiency.* N Engl J Med, 2004. **350**(13): p. 1296-303.
94. Saugstad, O.D., *et al*., *Novel mutations in the gene encoding ATP binding cassette protein member A3 (ABCA3) resulting in fatal neonatal lung disease.* Acta Paediatr, 2007. **96**(2): p. 185-90.
95. Citti, A., *et al*., *Ultrastructural characterization of genetic diffuse lung diseases in infants and children: a cohort study and review.* Ultrastruct Pathol, 2013. **37**(5): p. 356-65.

96. Carrera, P., *et al*., *Null ABCA3 in humans: large homozygous ABCA3 deletion, correlation to clinical-pathological findings.* Pediatr Pulmonol, 2014. **49**(3): p. E116-20.
97. Peca, D., *et al*., *Clinical and ultrastructural spectrum of diffuse lung disease associated with surfactant protein C mutations.* Eur J Hum Genet, 2015. **23**(8): p. 1033-41.
98. Beers, M.F. and S. Mulugeta, *The biology of the ABCA3 lipid transporter in lung health and disease.* Cell Tissue Res, 2017. **367**(3): p. 481-493.
99. Maly, J., *et al*., *Respiratory failure in a term newborn due to compound heterozygous ABCA3 mutation: the case report of another lethal variant.* J Perinatol, 2014. **34**(12): p. 951-3.
100. Jackson, T., *et al*., *Respiratory failure in a term infant with cis and trans mutations in ABCA3.* J Perinatol, 2015. **35**(3): p. 231-2.
101. Piersigilli, F., *et al*., *New ATP-binding cassette A3 mutation causing surfactant metabolism dysfunction pulmonary type 3.* Pediatr Int, 2015. **57**(5): p. 970-4.
102. Rezaei, F., *et al*., *Novel Mutation in the ATP-Binding Cassette Transporter A3 (ABCA3) Encoding Gene Causes Respiratory Distress Syndrome in A Term Newborn in Southwest Iran.* Iran J Pediatr, 2016. **26**(2): p. e2493.
103. AlAnazi, A., *et al*., *The most frequent ABCA3 nonsense mutation -p.Tyr1515* (Y1515X) causing lethal neonatal respiratory failure in a term neonate.* Ann Thorac Med, 2017. **12**(3): p. 213-215.
104. Akil, N. and A.J. Fischer, *Surfactant deficiency syndrome in an infant with a C-terminal frame shift in ABCA3: A case report.* Pediatr Pulmonol, 2018. **53**(5): p. E12-E14.
105. Mitsiakos, G., *et al*., *A New ABCA3 Gene Mutation c.3445G>A (p.Asp1149Asn) as a Causative Agent of Newborn Lethal Respiratory Distress Syndrome.* Medicina (Kaunas), 2019. **55**(7).
106. Wambach, J.A., *et al*., *Genotype-phenotype correlations for infants and children with ABCA3 deficiency.* Am J Respir Crit Care Med, 2014. **189**(12): p. 1538-43.
107. Hime, N.J., *et al*., *Childhood interstitial lung disease: A systematic review.* Pediatr Pulmonol, 2015. **50**(12): p. 1383-92.
108. Nathan, N., K. Borensztajn, and A. Clement, *Genetic causes and clinical management of pediatric interstitial lung diseases.* Curr Opin Pulm Med, 2018. **24**(3): p. 253-259.
109. Griese, M., *Chronic interstitial lung disease in children.* Eur Respir Rev, 2018. **27**(147).
110. Saddi, V., *et al*., *Childhood interstitial lung diseases in immunocompetent children in Australia and New Zealand: a decade's experience.* Orphanet J Rare Dis, 2017. **12**(1): p. 133.
111. Nogee, L.M., *Genetics of pediatric interstitial lung disease.* Curr Opin Pediatr, 2006. **18**(3): p. 287-92.
112. Matsumura, Y., N. Ban, and N. Inagaki, *Aberrant catalytic cycle and impaired lipid transport into intracellular vesicles in ABCA3 mutants associated with nonfatal pediatric interstitial lung disease.* Am J Physiol Lung Cell Mol Physiol, 2008. **295**(4): p. L698-707.
113. Young, L.R., *et al*., *Usual interstitial pneumonia in an adolescent with ABCA3 mutations.* Chest, 2008. **134**(1): p. 192-5.
114. Kinting, S., *et al*., *Functional rescue of misfolding ABCA3 mutations by small molecular correctors.* Hum Mol Genet, 2018. **27**(6): p. 943-953.
115. Schindlbeck, U., *et al*., *ABCA3 missense mutations causing surfactant dysfunction disorders have distinct cellular phenotypes.* Hum Mutat, 2018. **39**(6): p. 841-850.

116. Winter, J., *et al*., *Neonatal respiratory insufficiency caused by an (homozygous) ABCA3-stop mutation: a systematic evaluation of therapeutic options.* Klin Padiatr, 2014. **226**(2): p. 53-8.
117. Kroner, C., *et al*., *Lung disease caused by ABCA3 mutations.* Thorax, 2017. **72**(3): p. 213-220.
118. El Boustany, P., *et al*., *Unusual long survival despite severe lung disease of a child with biallelic loss of function mutations in ABCA-3.* Respir Med Case Rep, 2018. **23**: p. 173-175.
119. Galietta, L.V., S. Jayaraman, and A.S. Verkman, *Cell-based assay for high-throughput quantitative screening of CFTR chloride transport agonists.* Am J Physiol Cell Physiol, 2001. **281**(5): p. C1734-42.
120. Carlile, G.W., *et al*., *Correctors of protein trafficking defects identified by a novel high-throughput screening assay.* Chembiochem, 2007. **8**(9): p. 1012-20.
121. Van Goor, F., *et al*., *Correction of the F508del-CFTR protein processing defect in vitro by the investigational drug VX-809.* Proc Natl Acad Sci U S A, 2011. **108**(46): p. 18843-8.
122. Ren, H.Y., *et al*., *VX-809 corrects folding defects in cystic fibrosis transmembrane conductance regulator protein through action on membrane-spanning domain 1.* Mol Biol Cell, 2013. **24**(19): p. 3016-24.
123. Ramsey, B.W., *et al*., *A CFTR potentiator in patients with cystic fibrosis and the G551D mutation.* N Engl J Med, 2011. **365**(18): p. 1663-72.
124. Davies, J.C., *et al*., *Efficacy and safety of ivacaftor in patients aged 6 to 11 years with cystic fibrosis with a G551D mutation.* Am J Respir Crit Care Med, 2013. **187**(11): p. 1219-25.
125. Hoppner, S., *et al*., *Quantification of volume and lipid filling of intracellular vesicles carrying the ABCA3 transporter.* Biochim Biophys Acta Mol Cell Res, 2017. **1864**(12): p. 2330-2335.
126. Tanaka, A.R., *et al*., *Effects of mutations of ABCA1 in the first extracellular domain on subcellular trafficking and ATP binding/hydrolysis.* J Biol Chem, 2003. **278**(10): p. 8815-9.
127. Kimura, Y., *et al*., *ATP hydrolysis-dependent multidrug efflux transporter: MDR1/P-glycoprotein.* Curr Drug Metab, 2004. **5**(1): p. 1-10.
128. Hashimoto, K., *et al*., *Trafficking and functional defects by mutations of the ATP-binding domains in MRP2 in patients with Dubin-Johnson syndrome.* Hepatology, 2002. **36**(5): p. 1236-45.
129. Aharoni, R., *et al*., *Assessing remyelination - metabolic labeling of myelin in an animal model of multiple sclerosis.* J Neuroimmunol, 2016. **301**: p. 7-11.
130. Jao, C.Y., *et al*., *Metabolic labeling and direct imaging of choline phospholipids in vivo.* Proc Natl Acad Sci U S A, 2009. **106**(36): p. 15332-7.
131. Wittmann, T., *et al*., *Increased Risk of Interstitial Lung Disease in Children with a Single R288K Variant of ABCA3.* Mol Med, 2016. **22**: p. 183-191.
132. Zarbock, R., *et al*., *ABCA3 protects alveolar epithelial cells against free cholesterol induced cell death.* Biochim Biophys Acta, 2015. **1851**(7): p. 987-95.
133. Torrano, A.A., *et al*., *A fast analysis method to quantify nanoparticle uptake on a single cell level.* Nanomedicine (Lond), 2013. **8**(11): p. 1815-28.
134. Dohmen, L.C., *et al*., *Functional Validation of ABCA3 as a Miltefosine Transporter in Human Macrophages: IMPACT ON INTRACELLULAR SURVIVAL OF LEISHMANIA (VIANNIA) PANAMENSIS.* J Biol Chem, 2016. **291**(18): p. 9638-47.
135. Rodriguez-Gonzalez, A., *et al*., *Inhibition of choline kinase as a specific cytotoxic strategy in oncogene-transformed cells.* Oncogene, 2003. **22**(55): p. 8803-12.

136. Suwabe, A., R.J. Mason, and D.R. Voelker, *Temporal segregation of surfactant secretion and lamellar body biogenesis in primary cultures of rat alveolar type II cells.* Am J Respir Cell Mol Biol, 1991. **5**(1): p. 80-6.
137. Ekelund, L., *et al*., *Effect of cortisol on human fetal lung in organ culture: a biochemical, electron-microscopic and autoradiographic study.* Cell Tissue Res, 1975. **163**(3): p. 263-72.
138. Haldar, S., & Chattopadhyay, A. , *Application of NBD-Labeled Lipids in Membrane and Cell Biology*. 2012: Fluorescent Methods to Study Biological Membranes. p. 37–50.
139. Weng, C.J., *et al*., *The influence of NBD fluorescent probe on model membranes containing POPC and DPPC.* Mol Membr Biol, 2016. **33**(1-2): p. 23-28.
140. Loura, L.M., *et al*., *Effects of fluorescent probe NBD-PC on the structure, dynamics and phase transition of DPPC. A molecular dynamics and differential scanning calorimetry study.* Biochim Biophys Acta, 2008. **1778**(2): p. 491-501.
141. Weichert, N., *et al*., *Some ABCA3 mutations elevate ER stress and initiate apoptosis of lung epithelial cells.* Respir Res, 2011. **12**: p. 4.
142. Rumin, J., *et al*., *The use of fluorescent Nile red and BODIPY for lipid measurement in microalgae.* Biotechnol Biofuels, 2015. **8**: p. 42.
143. Govender, T., *et al*., *BODIPY staining, an alternative to the Nile Red fluorescence method for the evaluation of intracellular lipids in microalgae.* Bioresour Technol, 2012. **114**: p. 507-11.
144. Cabanelas, I.T.D., *et al*., *Rapid method to screen and sort lipid accumulating microalgae.* Bioresour Technol, 2015. **184**: p. 47-52.
145. Das, A.R., *et al*., *Intracellular surfactant removal from phagocytized minerals: development of a fluorescent method using a BODIPY-labeled phospholipid.* Inhal Toxicol, 2000. **12**(8): p. 765-81.
146. Diemel, R.V., *et al*., *In vitro and in vivo intrapulmonary distribution of fluorescently labeled surfactant.* Crit Care Med, 2002. **30**(5): p. 1083-90.
147. Diemel, R.V., *et al*., *Functional tests for the characterization of surfactant protein B (SP-B) and a fluorescent SP-B analog.* Arch Biochem Biophys, 2001. **385**(2): p. 338-47.
148. Cabre, E.J., *et al*., *Homo- and hetero-oligomerization of hydrophobic pulmonary surfactant proteins SP-B and SP-C in surfactant phospholipid membranes.* J Biol Chem, 2018. **293**(24): p. 9399-9411.
149. Luo, Z., *et al*., *Optical molecular imaging approach for rapid assessment of response of individual cancer cells to chemotherapy.* J Biomed Opt, 2012. **17**(10): p. 106006.
150. Luo, Z., *et al*., *High-resolution optical molecular imaging of changes in choline metabolism in oral neoplasia.* Transl Oncol, 2013. **6**(1): p. 33-41.
151. Paper, J.M., T. Mukherjee, and K. Schrick, *Bioorthogonal click chemistry for fluorescence imaging of choline phospholipids in plants.* Plant Methods, 2018. **14**: p. 31.
152. Di Guilmi, A.M., *et al*., *Specific and spatial labeling of choline-containing teichoic acids in Streptococcus pneumoniae by click chemistry.* Chem Commun (Camb), 2017. **53**(76): p. 10572-10575.
153. Pasternak, C.A. and J.J. Bergeron, *Turnover of mammalian phospholipids. Stable and unstable components in neoplastic mast cells.* Biochem J, 1970. **119**(3): p. 473-80.
154. Macara, I.G., *Elevated phosphocholine concentration in ras-transformed NIH 3T3 cells arises from increased choline kinase activity, not from phosphatidylcholine breakdown.* Mol Cell Biol, 1989. **9**(1): p. 325-8.

155. Lu, W.J., *et al*., *ATP-Binding Cassette Transporter VcaM from Vibrio cholerae is Dependent on the Outer Membrane Factor Family for Its Function.* Int J Mol Sci, 2018. **19**(4).
156. Kluth, M., *et al*., *A mutation within the extended X loop abolished substrate-induced ATPase activity of the human liver ATP-binding cassette (ABC) transporter MDR3.* J Biol Chem, 2015. **290**(8): p. 4896-907.
157. Bosnjak, I., *et al*., *First evidence of the P-glycoprotein gene expression and multixenobiotic resistance modulation in earthworm.* Arh Hig Rada Toksikol, 2014. **65**(1): p. 67-75.
158. Ishiguro, N., *et al*., *Decreased biosynthesis of lung surfactant constituent phosphatidylcholine due to inhibition of choline transporter by gefitinib in lung alveolar cells.* Pharm Res, 2008. **25**(2): p. 417-27.
159. Voelker, D.R. and F. Snyder, *Subcellular site and mechanism of synthesis of disaturated phosphatidylcholine in alveolar type II cell adenomas.* J Biol Chem, 1979. **254**(17): p. 8628-33.
160. Delahunty, T.J. and J.M. Johnston, *The incorporation of choline into disaturated phosphatidylcholine in the microsomal, lamellar body, and surfactant fractions of hamster lung tissue.* Can J Biochem, 1981. **59**(6): p. 436-9.
161. Sanchez-Lopez, E., *et al*., *Choline kinase inhibition induces exacerbated endoplasmic reticulum stress and triggers apoptosis via CHOP in cancer cells.* Cell Death Dis, 2013. **4**: p. e933.
162. Rodriguez-Gonzalez, A., *et al*., *Inhibition of choline kinase renders a highly selective cytotoxic effect in tumour cells through a mitochondrial independent mechanism.* Int J Oncol, 2005. **26**(4): p. 999-1008.
163. Ramirez de Molina, A., *et al*., *Choline kinase is a novel oncogene that potentiates RhoA-induced carcinogenesis.* Cancer Res, 2005. **65**(13): p. 5647-53.
164. Wnetrzak, A., K. Latka, and P. Dynarowicz-Latka, *Interactions of alkylphosphocholines with model membranes-the Langmuir monolayer study.* J Membr Biol, 2013. **246**(6): p. 453-66.
165. Carrasco, M.P., *et al*., *Hexadecylphosphocholine interferes with the intracellular transport of cholesterol in HepG2 cells.* FEBS J, 2008. **275**(8): p. 1675-86.
166. Geilen, C.C., T. Wieder, and W. Reutter, *Hexadecylphosphocholine inhibits translocation of CTP:choline-phosphate cytidylyltransferase in Madin-Darby canine kidney cells.* J Biol Chem, 1992. **267**(10): p. 6719-24.
167. Fisher, A.B., A. Chander, and J. Reicherter, *Uptake and degradation of natural surfactant by isolated rat granular pneumocytes.* Am J Physiol, 1987. **253**(6 Pt 1): p. C792-6.
168. Li, Y., *et al*., *Metabolic labelling of choline phospholipids probes ABCA3 transport in lamellar bodies.* Biochim Biophys Acta Mol Cell Biol Lipids, 2019. **1864**(12): p. 158516.
169. Quinlivan, V.H., *et al*., *An HPLC-CAD/fluorescence lipidomics platform using fluorescent fatty acids as metabolic tracers.* J Lipid Res, 2017. **58**(5): p. 1008-1020.
170. Otis, J.P., *et al*., *Dietary cholesterol and apolipoprotein A-I are trafficked in endosomes and lysosomes in the live zebrafish intestine.* Am J Physiol Gastrointest Liver Physiol, 2019. **316**(3): p. G350-G365.
171. Modzel, M., F.W. Lund, and D. Wustner, *Synthesis and Live-Cell Imaging of Fluorescent Sterols for Analysis of Intracellular Cholesterol Transport.* Methods Mol Biol, 2017. **1583**: p. 111-140.
172. Sanders, R.L., R.J. Hassett, and A.E. Vatter, *Isolation of lung lamellar bodies and their conversion to tubular myelin figures in vitro.* Anat Rec, 1980. **198**(3): p. 485-501.
173. Gil, J. and O.K. Reiss, *Isolation and characterization of lamellar bodies and tubular myelin from rat lung homogenates.* J Cell Biol, 1973. **58**(1): p. 152-71.

174. Chander, A., *et al*., *Isolation of lamellar bodies from rat granular pneumocytes in primary culture.* Biochim Biophys Acta, 1983. **753**(1): p. 119-29.

175. Zehner, M., *et al*., *Intraendosomal flow cytometry: a novel approach to analyze the protein composition of antigen-loaded endosomes.* Eur J Immunol, 2012. **42**(8): p. 2187-90.

176. Degtyarev, M., M. Reichelt, and K. Lin, *Novel quantitative autophagy analysis by organelle flow cytometry after cell sonication.* PLoS One, 2014. **9**(1): p. e87707.

177. Chasan, A.I., *et al*., *Isolation of a specialized, antigen-loaded early endosomal subpopulation by flow cytometry.* Methods Mol Biol, 2013. **960**: p. 379-388.

178. Swain, R.J., *et al*., *Assessment of cell line models of primary human cells by Raman spectral phenotyping.* Biophys J, 2010. **98**(8): p. 1703-11.

179. Mao, P., *et al*., *Human alveolar epithelial type II cells in primary culture.* Physiol Rep, 2015. **3**(2).

180. Wu, J., *et al*., *Characterization of air-liquid interface culture of A549 alveolar epithelial cells.* Braz J Med Biol Res, 2017. **51**(2): p. e6950.

181. Ohlinger, K., *et al*., *Air-liquid interface culture changes surface properties of A549 cells.* Toxicol In Vitro, 2019. **60**: p. 369-382.